

Metrology for spatial interferometry IV

Yekta Gürsel

Jet Propulsion Laboratory
California Institute of Technology
4800 oak Grove Dr., Pasadena, CA 91109

ABSTRACT

The proposed Space Interferometry Mission (SIM) spacecraft carries high resolution stellar interferometers for micro-arc-second accuracy astrometric measurements. These stellar interferometers require picometer accuracy one dimensional metrology gauges, surface metrology gauges and 3-dimensional metrology gauges. The absolute metrology gauges required by these interferometers can be considerably less accurate due to the careful design of the astrometric interferometers on the spacecraft.

Open-faced, hollow corner cube retro-reflectors are used as fiducials in the one-dimensional relative and absolute metrology gauges and the 3-dimensional metrology gauge. The diffraction caused by the assembly and the component defects of these hollow retro-reflectors affects the accuracy of these metrology gauges. A simulation quantifying some of the effects of the component and assembly defects of hollow retro-reflectors on the accuracy of a picometer linear metrology gauge is presented.

An auto-aligning, 3-dimensional metrology gauge constructed using the sub-picometer linear metrology gauges was described in earlier papers. The functioning automatic alignment and the sub-nanometer, in-air tracking results from this 3-dimensional metrology gauge are presented.

1. INTRODUCTION

Very high resolution spatial interferometry requires picometer level one-dimensional metrology, surface metrology and 3-dimensional metrology. The absolute distance measurements with accuracies of only 1 part in a million are required due to the careful design of spacecraft like the proposed Space Interferometry Mission (SIM), carrying high resolution stellar interferometers.

In four previous papers^{2,3,4} a relative metrology gauge capable of sub-picometer accuracy, a surface metrology gauge with sub-nanometer repeatability, and a completely functional absolute metrology gauge with a repeatability of nearly of 1 part in 10^6 , and initial test results from a 3-dimensional metrology gauge were described.

The 3-dimensional gauge described had just been constructed last year. To test its hardware and its software I had performed high speed tracking tests where the air turbulence and the ambient vibrations did not have a major effect of the tracking performance. These tests had verified that the gauge was functional and ready to be placed in its vacuum chamber.

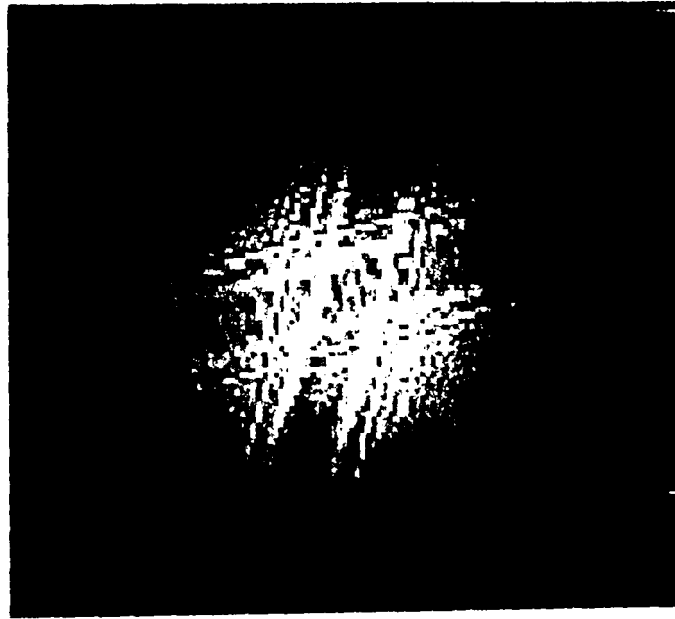
These gauges use hollow corner cube retro-reflectors as fiducial points. The laser beams from the gauge heads strike the corner of the retro-reflector. This corner is the most ill-defined area of the retro-reflector due to manufacturing and assembly defects. Strong diffracted fields caused by these defects alter the incident beam, resulting in a reflected beam that bears little resemblance to it. At the end of the last paper¹, actual pictures of a beam incident on a highly-accurate retro-reflector and the reflected beam from the same retro-reflector were shown.

In what follows, I will first describe a simulation showing exactly how these diffracted fields arise and quantifying their effects on the accuracy of the one-dimensional metrology gauges using these retro-reflectors as fiducials.

Next, the in-air, auto-alignment results from the linear gauges of the 3-r) metrology gauge is presented.

Finally, the in-air, actual tracking results from the 3-dimensional metrology gauge for extended measurement corner cube motions are presented. The detected motions allow the crudely measured initial positions of the measurement heads to be refined by requiring total agreement between all triangulations.

Figure 1: Computed diffraction pattern of the reflected beam from a hollow retro-reflector



2. 3-1) METROLOGY GAUGE

2.1. Corner Cube Induced Aberrations

In the previous paper⁴, the effect of a highly accurate, hollow retro-reflector on a nearly Gaussian, incident beam was experimentally measured by digitizing the images of the incident and the reflected beams. The pictured diffraction patterns hint at the cause of the beam profile damage. It is most likely to be caused by the gaps between the edges of the front surface mirrors that form the hollow retro-reflector.

In order to determine the exact cause of these diffraction patterns, I set up a simulation using the JPL developed MACOS⁵ program. In this simulation a Gaussian beam with a 3 mm waist radius impinges on a hollow retro-reflector with gaps of the order of 120 microns between the edges of its front surface mirrors, with a surface warpage of the order of $\lambda/10$ on the surface of these mirrors and with a slight deviation from orthogonality of the order of 1 arc-second between the mirror faces. The area of the beam is covered by a 256 x 256 grid of points. The simulation is performed with unpolarized light beams. The effects of polarization will be examined in a subsequent paper.

Fig. 1 shows the computed reflected beam at a wavelength of 632.8 nm at a distance comparable to the one in the experiment described in my previous paper⁴. All basic features of the observed diffraction pattern are present in the computed beam. As a matter of fact, one can adjust the parameters described above to make the two pictures as similar to each other as possible, deducing approximations to the actual corner cube parameters in the process.

The next step is to estimate the effects of these diffraction patterns on the accuracy of the linear metrology gauges. Obviously, if the beams never move relative to the retro-reflectors and they never change size, these diffraction patterns do not change the accuracy. In realistic experimental configurations, these conditions are never satisfied. Dithering that moves the beam on the surface of the cube by large amounts is used to auto-align the one-dimensional metrology gauge.

A simulation that closely approximates a one-dimensional metrology gauge is set up by placing two corner cube retro-reflectors 10.44 meters apart. A reference Gaussian beam travels a short distance of the order of 10 cm and impinges on a photo-detector. The monitor beam takes a roundtrip between the retro-reflectors and then interferes with the reference beam on the photo-detector. The beam and the corner cube parameters are identical to the ones in the previous simulation, with the exception of the wavelength of light. It is 1319 nm in this simulation.

In order to quantify effects of beam wavefront distortion on the detected phase, I define a concept known as

“tile orthogonal wavefront”⁶. Let A be a near Gaussian complex, reference wavefront that does not travel between the corner cubes. Let B be another near Gaussian, complex wavefront that takes a round trip between the corner cubes and then returns to the detection location. A and B are assumed to have the same polarization, even after tile roundtrip.

At the detector, nearly equal parts of A and B interfere with each other due to the design of the heterodyne gauge. The interference is accomplished by computing the integrated absolute magnitude of the sum of the two wavefronts.

$$Interference = \langle |\alpha A + \beta B|^2 \rangle = \langle (\alpha A + \beta B) (\alpha A + \beta B)^* \rangle, \quad (1)$$

where $\langle \rangle$ denotes time average and spatial integration over the intersection of the bounded supports of the entire wavefronts A and B , and α, β are constants that are determined by the details of the detection mechanism. In a heterodyne interferometer, α is nearly equal to β in magnitude. Eq. (1) leads to:

$$Interference = |\alpha|^2 \langle |A|^2 \rangle + |\beta|^2 \langle |B|^2 \rangle + \alpha\beta^* \langle AB^* \rangle + \beta\alpha^* \langle BA^* \rangle. \quad (2)$$

It is clear that the interference is produced by the term $\langle AB^* \rangle$ and its complex conjugate. If this term vanishes, there is no interference between these two wavefronts. I define the orthogonal part B_o of the wavefront B to a given reference wavefront A as:

$$B_o = B - [\langle BA^* \rangle / \langle |A|^2 \rangle] A. \quad (3)$$

The parallel part B_p of the wavefront B to the given reference wavefront A is defined as:

$$B_p = [\langle BA^* \rangle / \langle |A|^2 \rangle] A. \quad (4)$$

Note that $B = B_o + B_p$, $\langle |B|^2 \rangle = \langle |B_o|^2 \rangle + \langle |B_p|^2 \rangle$ and $\langle AB_o^* \rangle = 0$, indicating that only B_p contributes to the detected fringe.

The magnitude of the complex number $[\langle BA^* \rangle / \langle |A|^2 \rangle]$ is related to the “fringe contrast”, and its phase apart from the propagation phase $2kL$ where k is the wave number of the propagating wave and L is the one way separation between the corner cubes, indicates the “extra phase shift” acquired due to diffraction damage at the corner cube retro-reflectors.

Fig. 2 shows the “extra phase shift” acquired as the retro-reflectors move transverse to the light beam.

Fig. 3 shows the intensity of the “orthogonal wavefront” that does not contribute to the detected phase, but reduces the “fringe contrast” at the extreme of the motion. The maximum amplitude of the initial Gaussian was 1. The spatial axes of the plot is labelled in pixels. In this simulation there were nearly 20 pixels to a mm.

Tile polarization of the reflected beam from the retro-reflectors also gets altered as the beam moves on the surface of the retro-reflectors. In the next sections, experimental data verifying this effect will be presented. An analysis to determine the exact nature of the observed effect is in progress.

2.2. Dithering and Auto-alignment

When the output of two one-dimensional relative metrology gauges monitoring the distance between two corners are compared to each other for small motions of the order of few wavelengths of light, there is usually a linear drift in the output comparison proportional to the misalignment of these linear gauges². In order to separate the actual distance change from the alignment drift, these gauges must to be aligned automatically parallel to the line connecting the corners of the corner cube.

Figure 2: The effect of corner cube imperfections on the detected phase

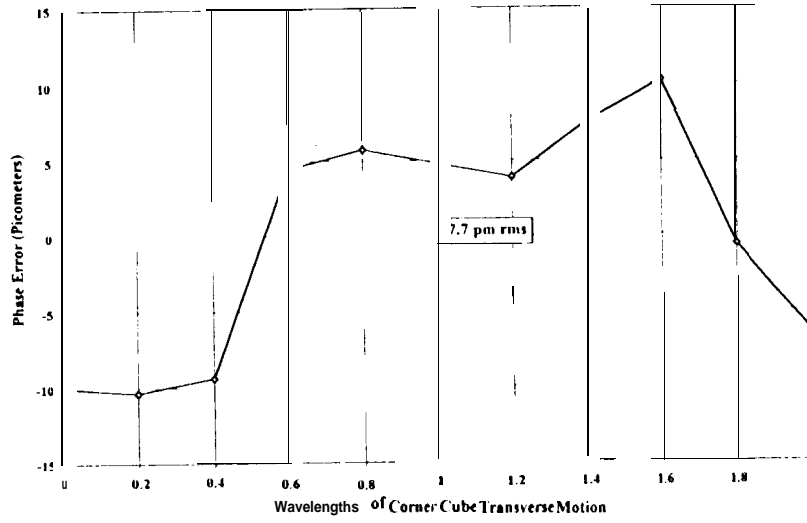


Figure 3: The intensity of the reflected orthogonal wavefront

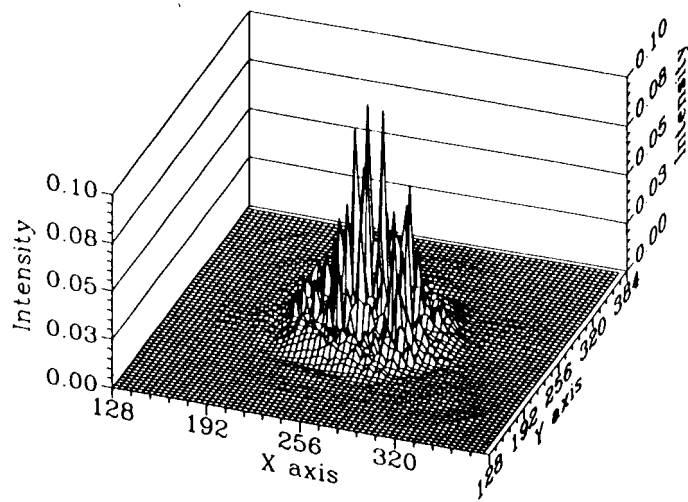
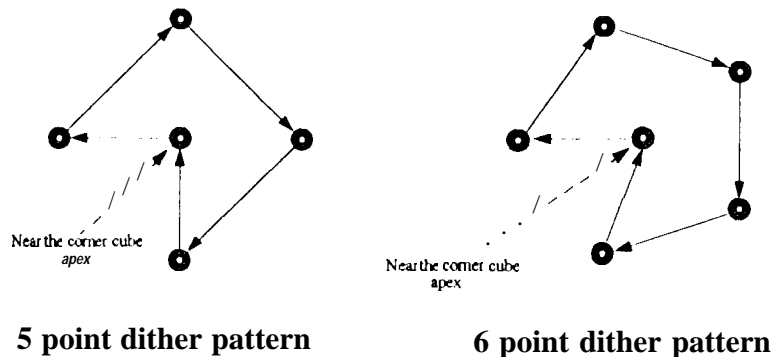


Figure 4: The five and six point dithering patterns



The gauge signals themselves can be used to perform this alignment. It is very easy to geometrically prove that the line connecting the corners of the two ideal corner cubes, spans the maximum distance between the cubes. Any other line segment bounded by the corner cube surfaces that is at an angle to line connecting the corners is shorter.

When the beam launcher cube that controls the direction of the beam between the corner cubes is moved around the line connecting the corners of the corner cubes, the measured distance falls on a symmetric paraboloid with apex in the direction of the line connecting the corners of the corner cubes for small motions on absolutely perfect retro-reflectors.

If the sides of the retro-reflectors are not exactly orthogonal to each other, a six sided figure that could vary between an inverted pyramid, a saddle shaped surface, and an upright pyramid gets added on to the symmetric paraboloid. To make the matters more difficult, the diffraction patterns caused by the gaps between the surfaces, the surface figure errors and the altered beam polarization further distort this already complicated figure pulling it away from the paraboloid and turning it into an asymmetric surface with multiple maxima.

However, by choosing sufficiently large dither amplitude, it is almost always possible to reach the symmetric tails of the "original" paraboloid. A fit to this paraboloid then points to its apex that is supposedly the optimum alignment position. If the corner cube retro-reflectors are very badly made, this alignment procedure will in general fail pointing to a phantom corner that does not follow the cube motion.

To test these ideas, the 3-D metrology apparatus that was described in my last paper³ is equipped with dithering heads that can move the beams away from the optimal alignment position by a maximum angular amplitude of about 50 to 100 micro-radians. The heads can be made to follow various dithering patterns the extent of which depend only on the available CPU speed of the controlling computers.

During the last year, the controlling computers were equipped with 33 MHz 68040 microprocessors, enabling me to perform five and six point dithered measurements while tracking the measurement corner cube in three dimensions. The dithering patterns are illustrated in Fig. 4.

The five point dither pattern was chosen to test how stationary the mapped surface was. If the surface rotates at all, the five point quadratic solution fails pointing the gauge in a bad direction. The six point solution will always find the extreme point of what it perceives to be actual corner. However, depending on the fine scale structure of the surface sampled, this deduced corner may not be the actual corner. The following figures illustrate the ideas presented with actual gauge output. The linear motion of the cube that is well tracked is removed from the graphs to make the small variations visible.

Figure 5: The Head #1 tracking without dithering

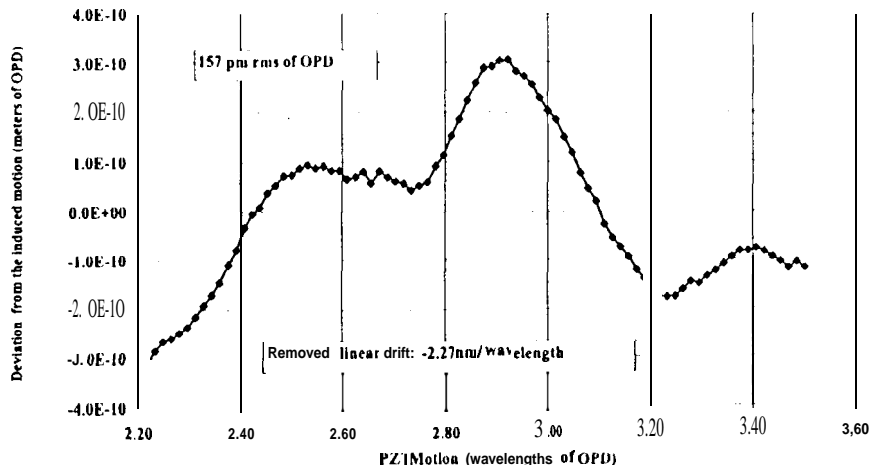


Fig. 5 shows one of the head outputs without dithering (central dithering position). There is a linear drift of -2.27 nm per wave of measurement corner cube motion.

Fig. 6 shows the same head output with five point dithering. There is no linear drift, but the five point solution occasionally fails, indicating that the quadratic surface that is being solved for is changing as the corner cube moves away from the head.

Fig. 7 shows another head scanning through the six point dither pattern as the corner cube moves away from the head. The measurements corresponding to different dither positions are plotted with different line styles.

Fig. 8 shows the six point solution to the dithered head motion as the retro-reflector moves away from the head. As clearly seen, the fitted position is very close to the central (no dither) position.

Recently, I upgraded the controlling computers to a much faster microprocessor that gave a 16 times speed increase. A complete 5×5 and 10×10 raster scans of the corner area of the measurement retro-reflector will be performed in the near future. The results of these scans will be presented in a subsequent paper.

2.3. The Effect of Retro-reflector Defects on Polarization

With the faster CPU, the 3-dimensional metrology gauge can move its measurement corner cube for about 25 microns using its pusher PZT in less than 10 minutes while collecting enough data to perform cyclic averaging and improve its one-dimensional resolution in vacuum to sub-picometers.

During one such run without dithering and in still air, I monitored the “self-interference” on one of the outer head signals as the middle servo head was controlling the motion. Since the outer heads see the measurement corner cube at an angle and the measurement corner cube is moving nearly perpendicular to the base plane, the outer head beam actually walks transversely on the measurement retro-reflector. If the beam polarization is affected by the diffraction and other defects of the corner cube, this should manifest itself as a change in the “self-interference” amplitude.

Fig. 9 shows “self-interference” observed by Head # 1 as a function of the motion of the measurement corner cube. The “one-wavelength of OPD” periodicity is as expected, and it is used to eliminate all traces of “self-interference”¹². However, the periodic change in the amplitude of this “self-interference” was unexpected. The period of the change in the amplitude is larger than 10 wavelengths of OPD and it does depend on the head that

Figure 6: The Head # 1 tracking with five point dithering

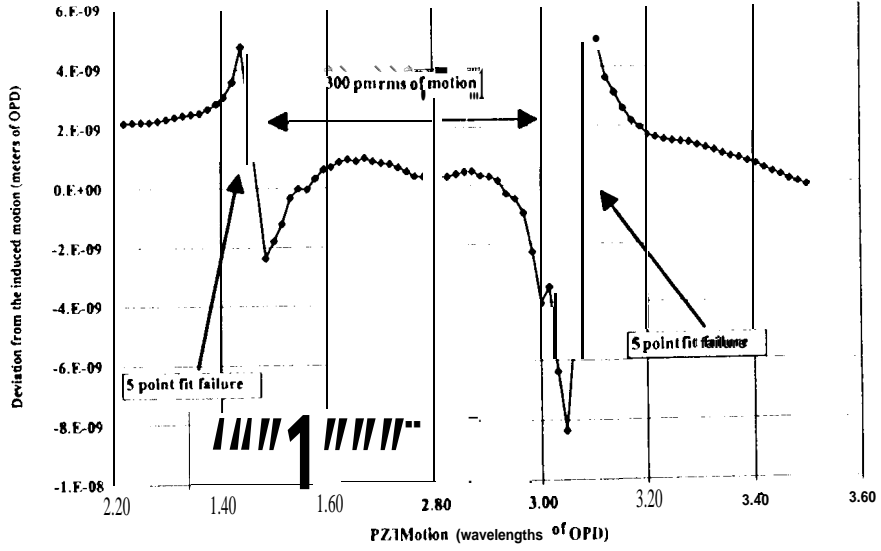


Figure 7: The Head #3 tracking with six point dithering

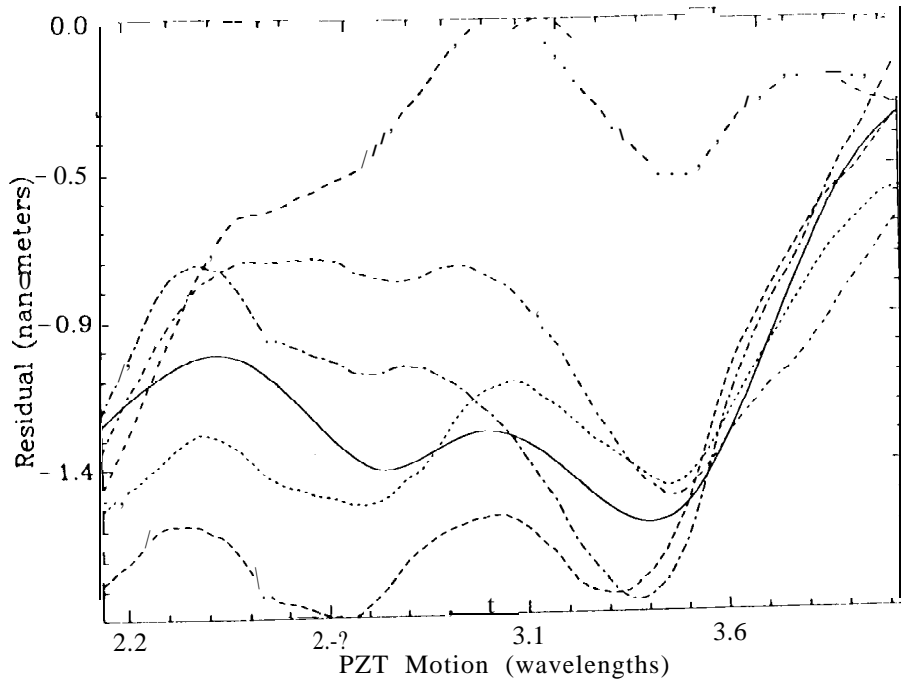


Figure 8: The Head #3 tracking the computed corner

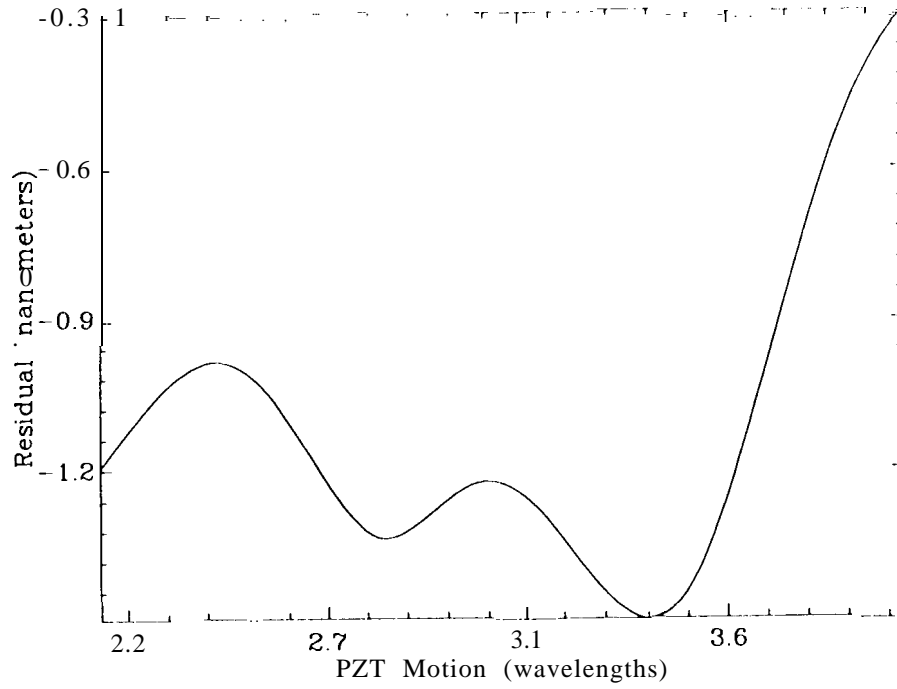


Figure 9: The self-interference observed by Head # 1

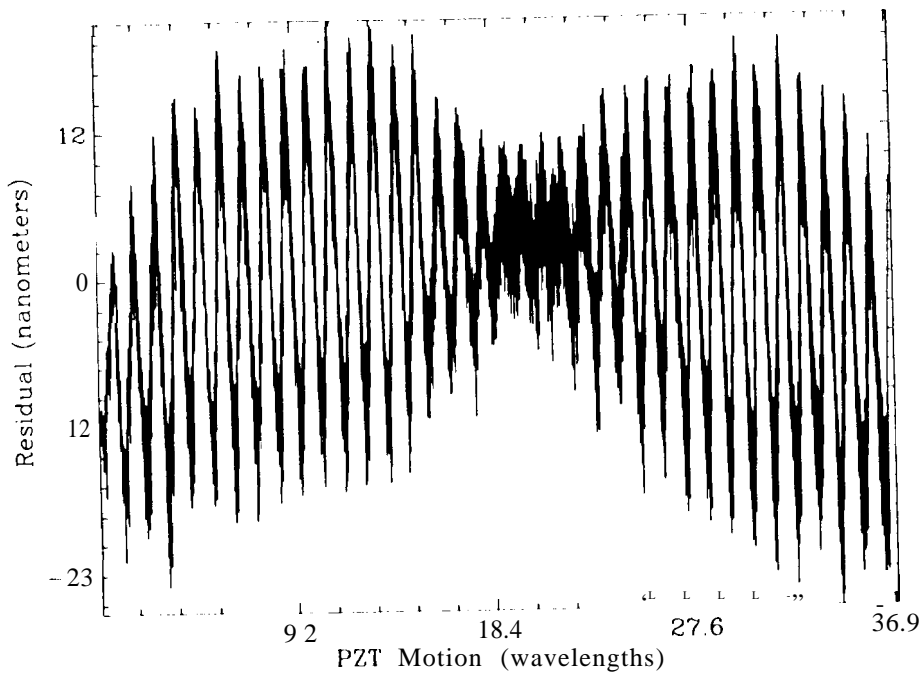
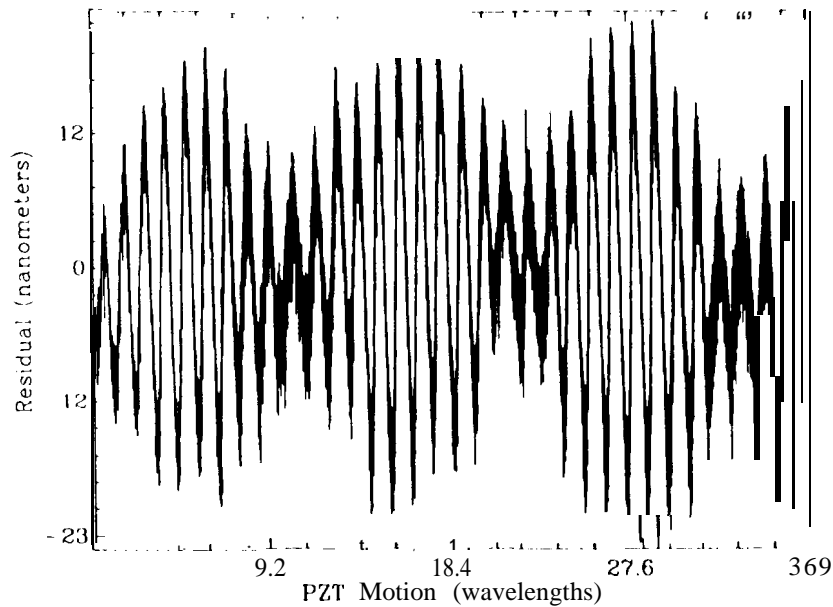


Figure 10: The self-interference observed by Head #1 after rotation



is performing the measurement as these see the corner cube at different angles. To make sure that the corner cube is responsible for the variations observed, I rotated the corner cube by nearly 90 degrees and repeated the measurement.

Fig. 10 shows ‘self-interference’ observed by Head # 1 as a function of the motion of the measurement corner cube after the rotation. The long term periodicity has changed. When the cube is rotated back to its original position, the amplitude pattern goes back to the one shown in Fig. 9 indicating that indeed the corner cube defects and the associated diffraction pattern are causing these changes in the polarization. Furthermore, if one rotates the cube so that another head is nearly at the same orientation with respect to tile cube as the previous one, a pattern variation nearly identical to that of the previous head appears.

The results of an analysis precisely determining the cause of these polarization changes will be reported in a subsequent paper.

2.4. The Complete Solution to Surveying in 3-dimensions in Euclidean Space

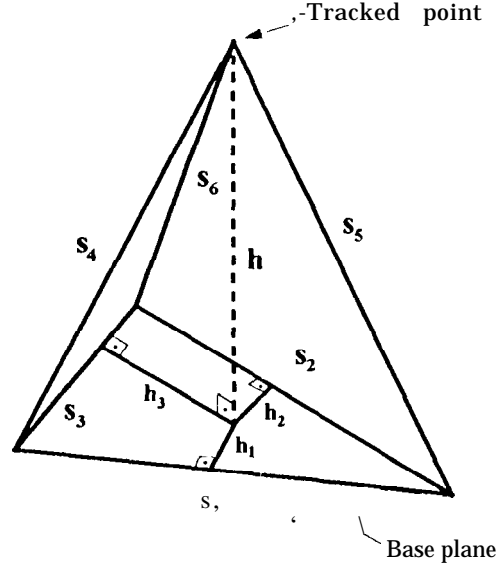
It is very well known that the position of a point in three dimensions can be precisely determined if the distances from this point to three other reference points that do not lie on a straight line are given.

In what follows, I will give analytic formulas that can be used in a hand-held calculator to compute the location of the tracked point with respect to 3 reference points when all the connecting distances are known. The author has not seen these formulas in the literature before.

Fig. 11 shows the geometrical arrangement. The lengths $s_1, s_2,$ and s_3 form the reference base triangle of an irregular tetrahedron. The lengths s_4, s_5 and s_6 connect the tracked point to the reference base triangle. h denotes the height of the tracked point as measured from the reference base triangle plane. The coordinate lengths h_1, h_2 and h_3 are the distances from the footprint of the height of the tetrahedron to the sides of the base reference triangle. The four numbers $h, h_1, h_2,$ and h_3 redundantly determine the position of the tracked point. Note that the coordinate lengths h_1 and h_2 and h_3 can be negative indicating that the footprint of the height is on the outside of the base triangle.

$$h^2 = (-s_1^2 s_6^4 - s_1^4 s_6^2 - s_2^2 s_4^4 - s_2^4 s_4^2 - s_3^2 s_5^4 - s_3^4 s_5^2 - s_1^2 s_2^2 s_3^2 + s_1^2 s_2^2 s_4^2 + s_1^2 s_2^2 s_6^2$$

Figure 11: The 3-dimensional surveying geometry



$$+s_1^2 s_3^2 s_5^2 + s_1^2 s_3^2 s_6^2 - s_1^2 s_4^2 s_5^2 + s_1^2 s_4^2 s_6^2 + s_1^2 s_5^2 s_6^2 + s_2^2 s_3^2 s_4^2 - s_2^2 s_3^2 s_5^2 + s_2^2 s_4^2 s_5^2 + s_2^2 s_4^2 s_6^2 - s_2^2 s_5^2 s_6^2 + s_3^2 s_4^2 s_5^2 - s_3^2 s_4^2 s_6^2 + s_3^2 s_5^2 s_6^2)/d^2, \quad (5)$$

where d is given by:

$$d^2 = -s_1^4 - s_2^4 - s_3^4 + 2s_1^2 s_2^2 + 2s_1^2 s_3^2 + 2s_2^2 s_3^2. \quad (6)$$

Note that $d = 4 * \text{Area of the triangle } (s_1, s_2, s_3)$. The coordinate lengths h_1, h_2 and h_3 are given by:

$$h_1 = (2s_1^2(s_2^2 + s_5^2 - s_6^2) - (s_1^2 + s_2^2 - s_3^2)(s_1^2 - s_4^2 + s_5^2))/2s_1 d, \quad (7)$$

$$h_2 = (2s_2^2(s_3^2 - s_4^2 + s_6^2) - (s_2^2 + s_3^2 - s_1^2)(s_2^2 - s_5^2 + s_6^2))/2s_2 d, \quad (8)$$

$$h_3 = (2s_3^2(s_2^2 - s_5^2 + s_6^2) - (s_2^2 + s_3^2 - s_1^2)(s_3^2 - s_4^2 + s_6^2))/2s_3 d, \quad (9)$$

These formulas are used in computing the tracking performance shown in the following section.

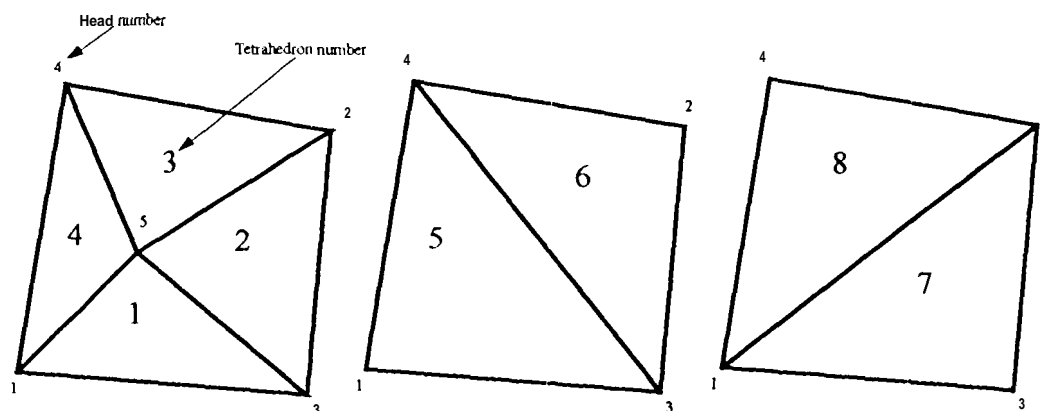
2.5. 3-dimensional Tracking in still Air

The five heads of the 3-dimensional metrology gauge together with the moving measurement corner cube form eight tetrahedra to monitor the motion of the measurement corner cube. Fig. 12 shows the base configurations of these tetrahedra.

In order to be able to derive the relative motion of the measurement corner cube, the positions of the base heads and the initial position of the measurement corner cube are crudely measured using rulers and digital photographs.

The 3-dimensional metrology gauge is operated in the non-dithered mode in still air inside the vacuum chamber on seismic isolation tracking the measurement corner cube for an approximate total motion of 25 microns, moving away from the plane of the heads. When the motion of the measurement corner cube is solved for each tetrahedra

Figure 12 The tetrahedra base configurations



using the formulas given above and the crude survey, the solutions for different tetrahedral differ by an amount linearly proportional to the motion of the measurement corner cube. This amount is about 8 to 10 nm per wavelength of OPD motion. Since the surveying is crude, a fit is performed using all available data to determine the final positions of the heads as well as the motion of the measurement corner cube by minimizing the difference in the motion reported by all eight tetrahedra.

In general, there are many local minima not all of which correspond to the physical positions of the heads and the measurement corner cube. Among these, the one closest to the crude survey position is regarded as the final tracking result. This approach is taken in order to test the gauge before the installation of the absolute metrology gauge on five of its beams.

The maximum base head coordinate difference after the solution is about four millimeters. The largest displacement is in the initial z position of the measurement corner cube, which is the most uncertain of the crudely surveyed lengths. This displacement is about 2.5 centimeters.

After the new solution is substituted, the disagreement between all eight tetrahedral is less than 2 nm peak for about 35 wavelengths of OPD motion in all coordinates of the measurement corner cube. For shorter stretches motion of the order of 10 wavelengths of OPD, the residual disagreement is well below a nanometer. A similar run with a rotated retro-reflector does agree with the results of the unrotated run within a few nm in the measurement retro-reflector position and head positions.

Figs. 13, 14, 15 show the detected motion of the measurement corner cube by tetrahedron # 1 in x, y and z coordinates.

Figs. 16, 17, 18 show difference between what is measured by tetrahedron # 1 and all the other tetrahedra in x, y and z coordinates respectively. The tetrahedral are distinguished by different line styles in the plots.

Due to index of refraction of the beam launcher cube in the measurement beams, the optical length measured by the heads does not correspond to the physical length measured by a ruler along the measurement beams. This causes outer heads to appear move out of the base plane by a about a millimeter. The absolute metrology system does offer a calibration of this amount as well.

The performance of the gauge with absolute metrology and with dithering in vacuum will be reported in the subsequent paper.

Figure 13: The x coordinate of the motion detected by tetrahedron #1

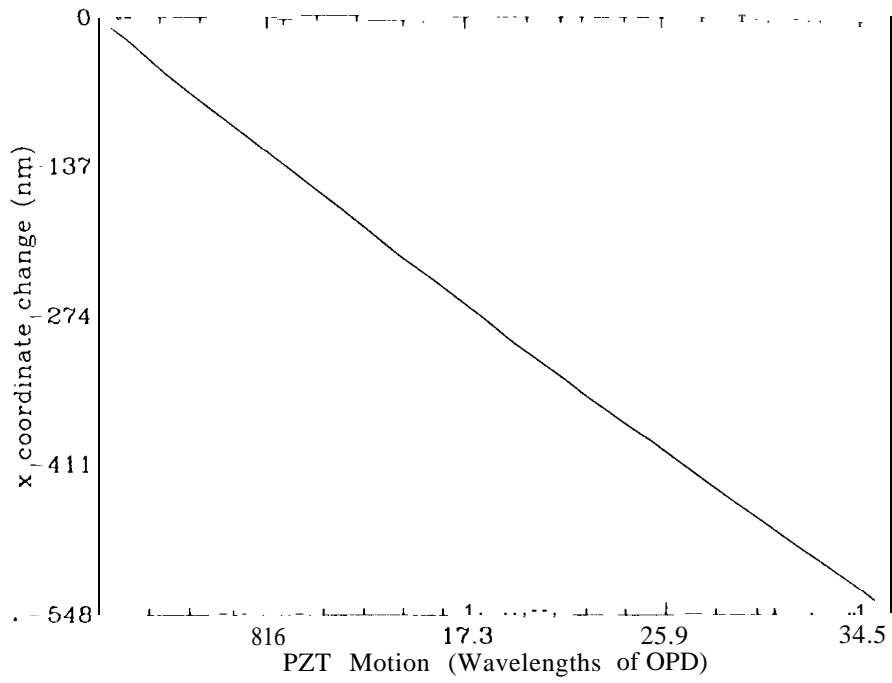


Figure 14: The y coordinate of the motion detected by tetrahedron # 1

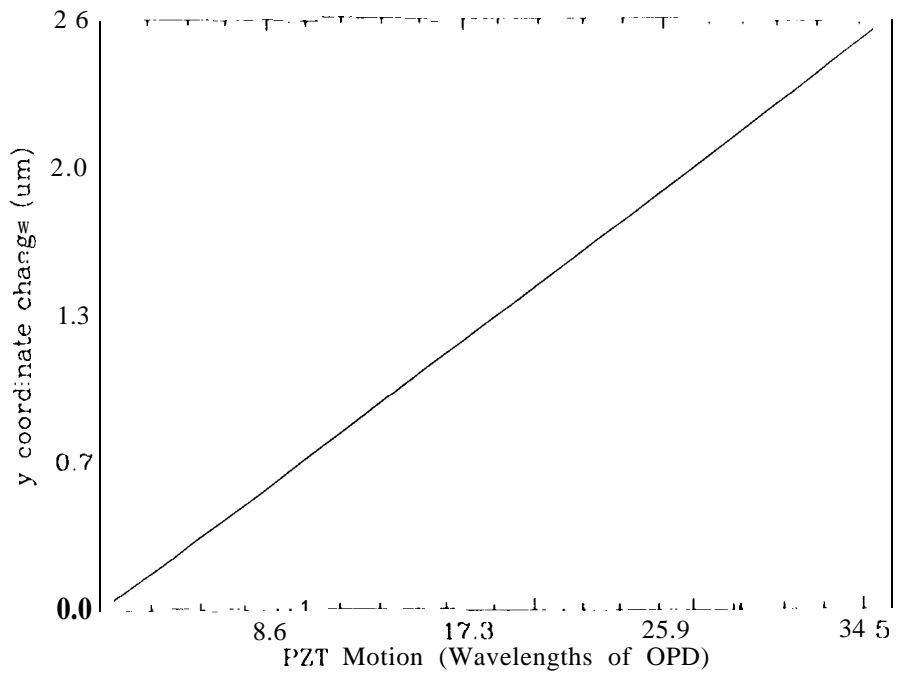


Figure 15: The z coordinate of the motion detected by tetrahedron #1

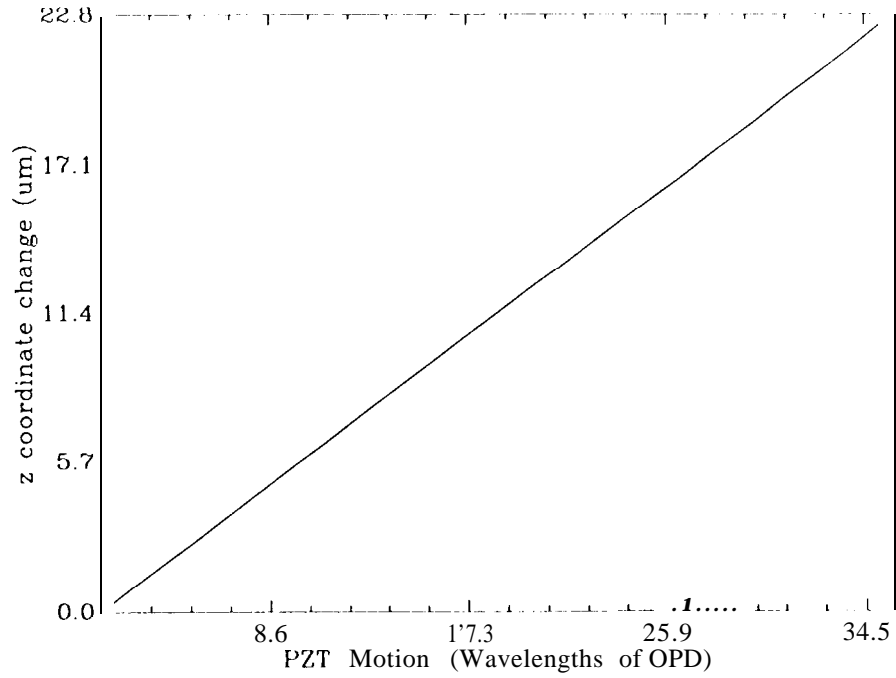


Figure 16: The x coordinate difference between tetrahedron #1 and all others

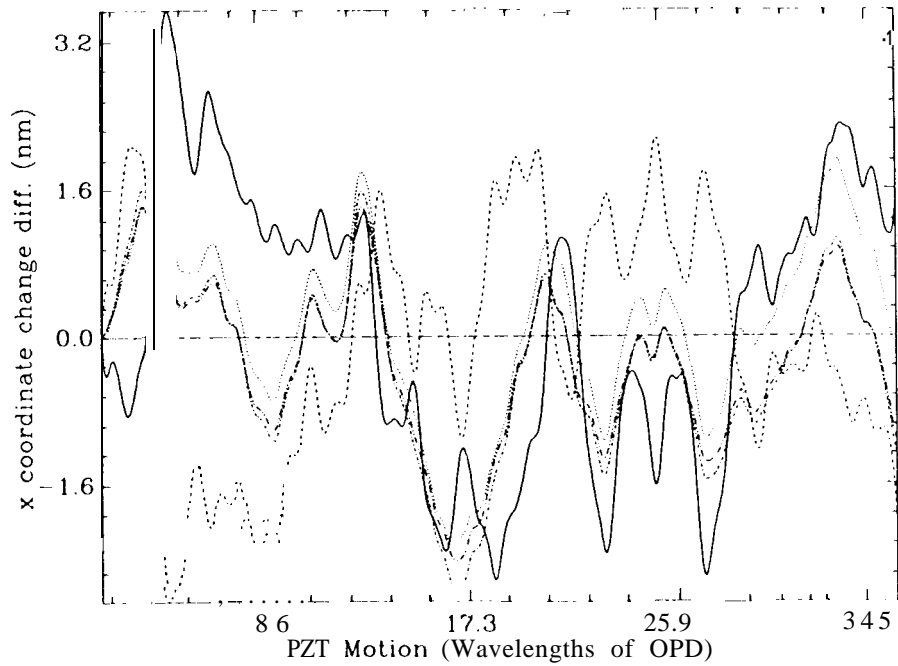


Figure ii: The y coordinate difference between tetrahedron #1 and all others

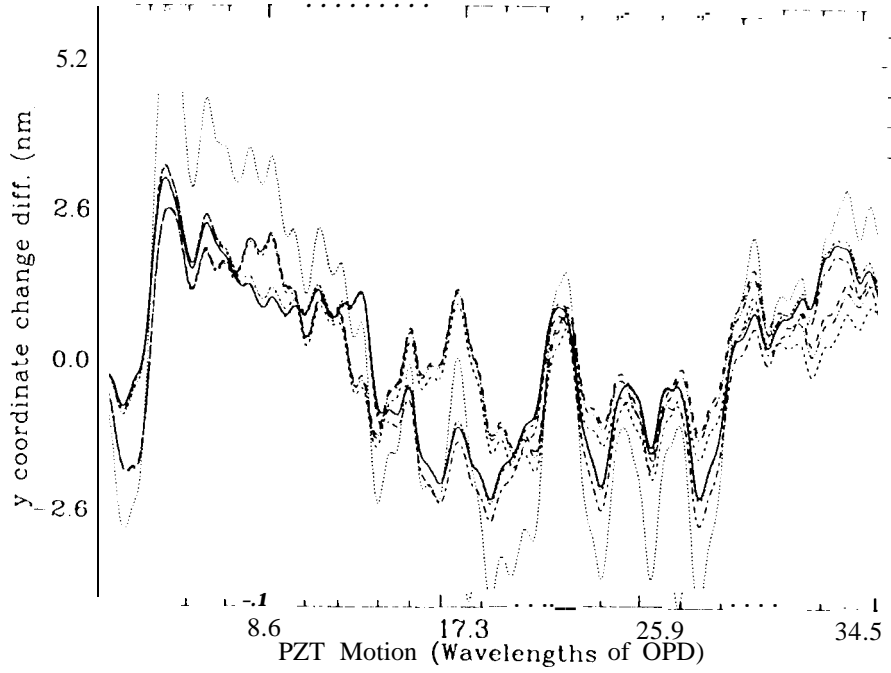
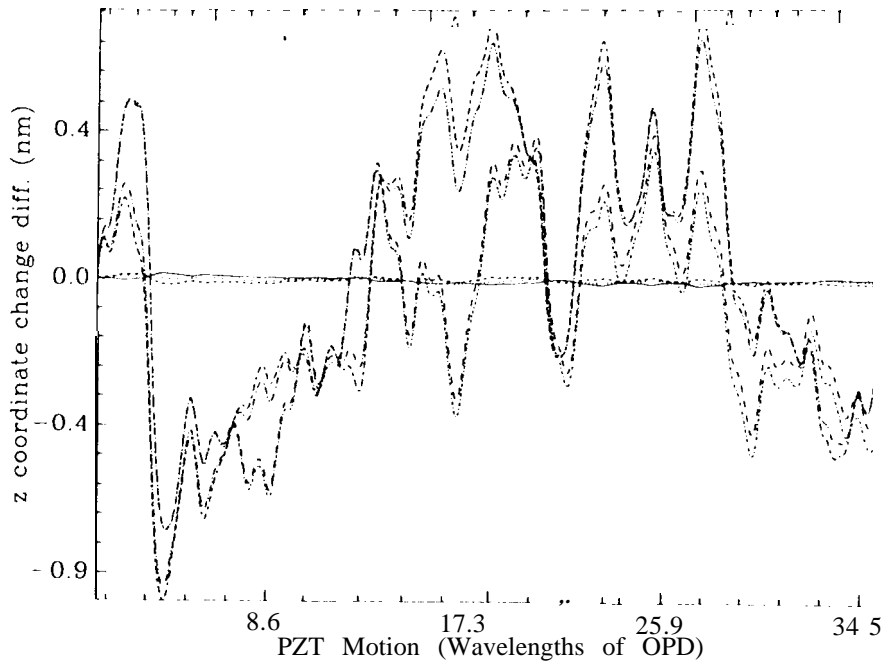


Figure 18: The z coordinate difference between tetrahedron # 1 and all others



3. SUMMARY

A simulation showing the effects of imperfect open-faced corner cube retro-reflectors on the measurement of laser beams is presented. For well-made corner cubes the detected phase error is less than 30 picometers as the cube moves transverse to the light beam for a few wavelengths of light. The effects of polarization are not considered in this simulation. The results of a simulation including polarization effects will be presented in a subsequent paper.

The heterodyne gauge data showing the effects of the corner cube defects on the polarization of the reflected beams is presented.

Analytical tracking formulas for 3-dimensional metrology are given. These are simple enough to implement on a hand-held calculator.

Finally, the tracking performance of the 3-dimensional metrology gauge in still air without absolute metrology, but with an initial crude survey is presented.

When the final head positions as well as the total motion is solved for using the data and the condition that all eight tetrahedra must agree on the motion, the residual disagreement between the tetrahedra is below a nanometer in x, y and z coordinates for short stretches of motion less than 10 wavelengths of OPD at 1319 nm. The total disagreement is below 2 nm peak for nearly 35 wavelengths of OPD motion at the same wavelength.

The maximum difference between the crude survey positions and the solved positions of the heads is about four millimeters. The largest displacement is in the initial z position of the measurement corner cube, that is the most uncertain of the crudely surveyed lengths. This displacement is about 2.5 centimeters.

The performance of the 3-dimensional metrology gauge in vacuum with absolute metrology will be reported in the subsequent paper.

4. ACKNOWLEDGEMENTS

I would like to thank M. Shao, J. Yu, and S. Shaklan for many fruitful discussions. I would also like to thank D. Redding for fixing the bugs I had run into while using MACOS. A. Carlson re-measured the base configuration with a ruler and pictures and indicated some discrepancies with the original crude survey. The research described was performed at the Jet Propulsion Laboratory, California Institute of Technology, under a contract with the National Aeronautics and Space Administration.

5. REFERENCES

1. Y. Gürsel. Laser metrology gauges for OS1, in *Proceedings of SPIE conference on Spaceborne Interferometry*, Vol. 1947, p. 188-197, 1993.
2. Y. Gürsel. Metrology for spatial interferometry, in *Proceedings of SPIE conference on Amplitude and Intensity Spatial Interferometry*, Vol. 2200, p. 27-34, 1994.
3. Y. Gürsel. Metrology for spatial interferometry II, in *Proceedings of SPIE conference on Spaceborne Interferometry II*, Vol. 2477, p. 240-258, 1995.
4. Y. Gürsel. Metrology for spatial interferometry I II, in *Proceedings of SPIE conference on Space Telescopes and Instruments IV*, Vol. 2807, p. 148-161, 1996.
5. Modeling and Analysis for Controlled Optical Systems, User Manual, *US Government Version*, Version 2.0, Jet Propulsion Laboratory, California Institute of Technology, January 25, 1996. No author is listed.
6. A similar definition to the one given in the text is used by the commercial GLAD diffraction analysis program.
7. Hines, B., Colavita, M. H., Wallace, J. K., Poulsen, A., "Sub-nanometer laser metrology - some techniques and models", in *Proceedings of High Resolution Imaging by Interferometry II*, ESO, Garching, Germany, 1991.

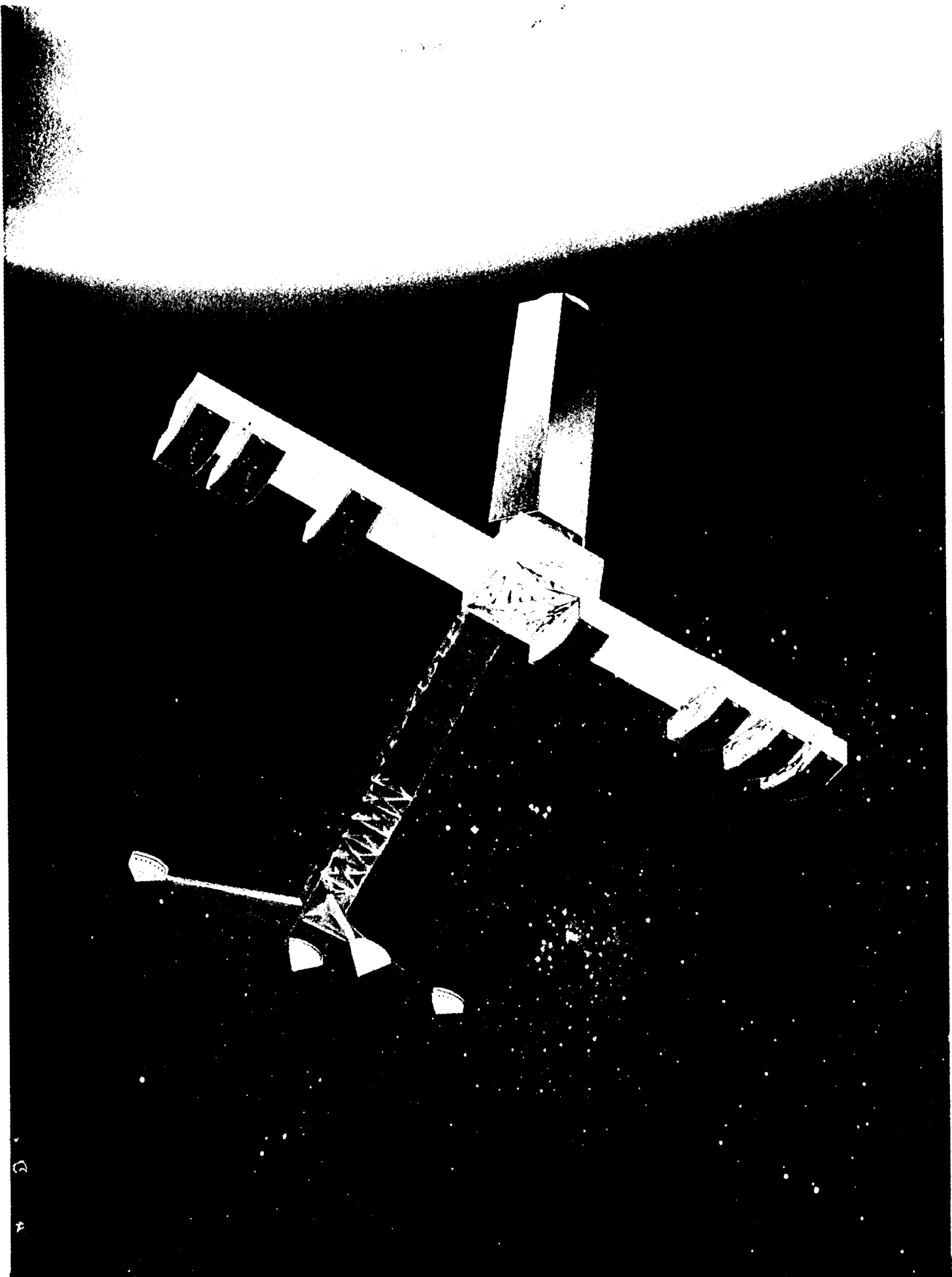
METROLOGY FOR SPATIAL INTERFEROMETRY IV

Yekta Gürsel

July 27,1997

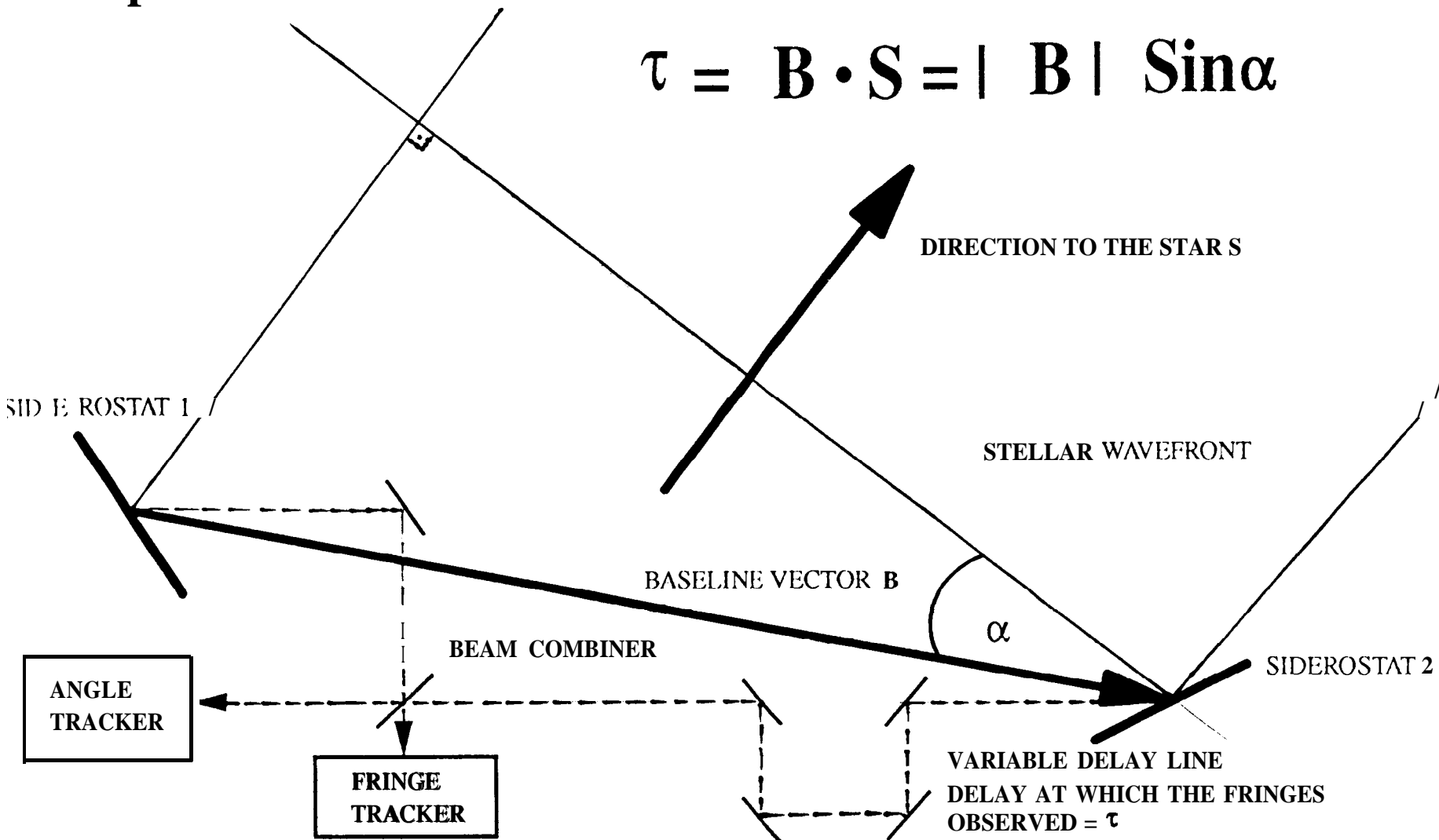


**Presentation to SPIE's International Symposium on
Optical Science, Engineering, and Instrumentation
Missions, Spacecraft and Instrumentation
for the New Millenium
San Diego, California**



INTRODUCTION

- **SIM requires a metrology system to measure the three dimensional baseline vector between any two of its siderostats and the distance from the beam combiner to the baseline end points.**



METROLOGY SYSTEMS

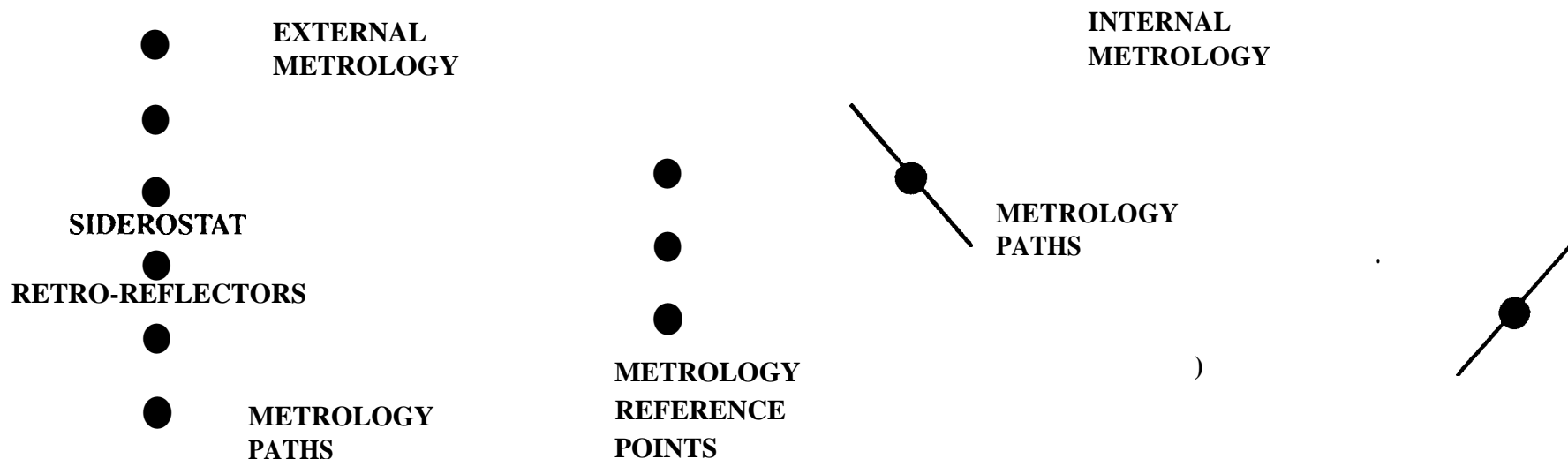
. **For astrometry, the instrument is completely described by four parameters:**

- . The baseline vector (3 components)
- . The delay offset

. **SIM uses laser metrology systems to monitor these parameters directly:**

- . Laser optical truss concept (External Metrology)
- . Delay-offset monitor (Internal Metrology)

. **3-D metrology accuracy of 25-250 picometers is required for 1-10 μ as astrometry.**

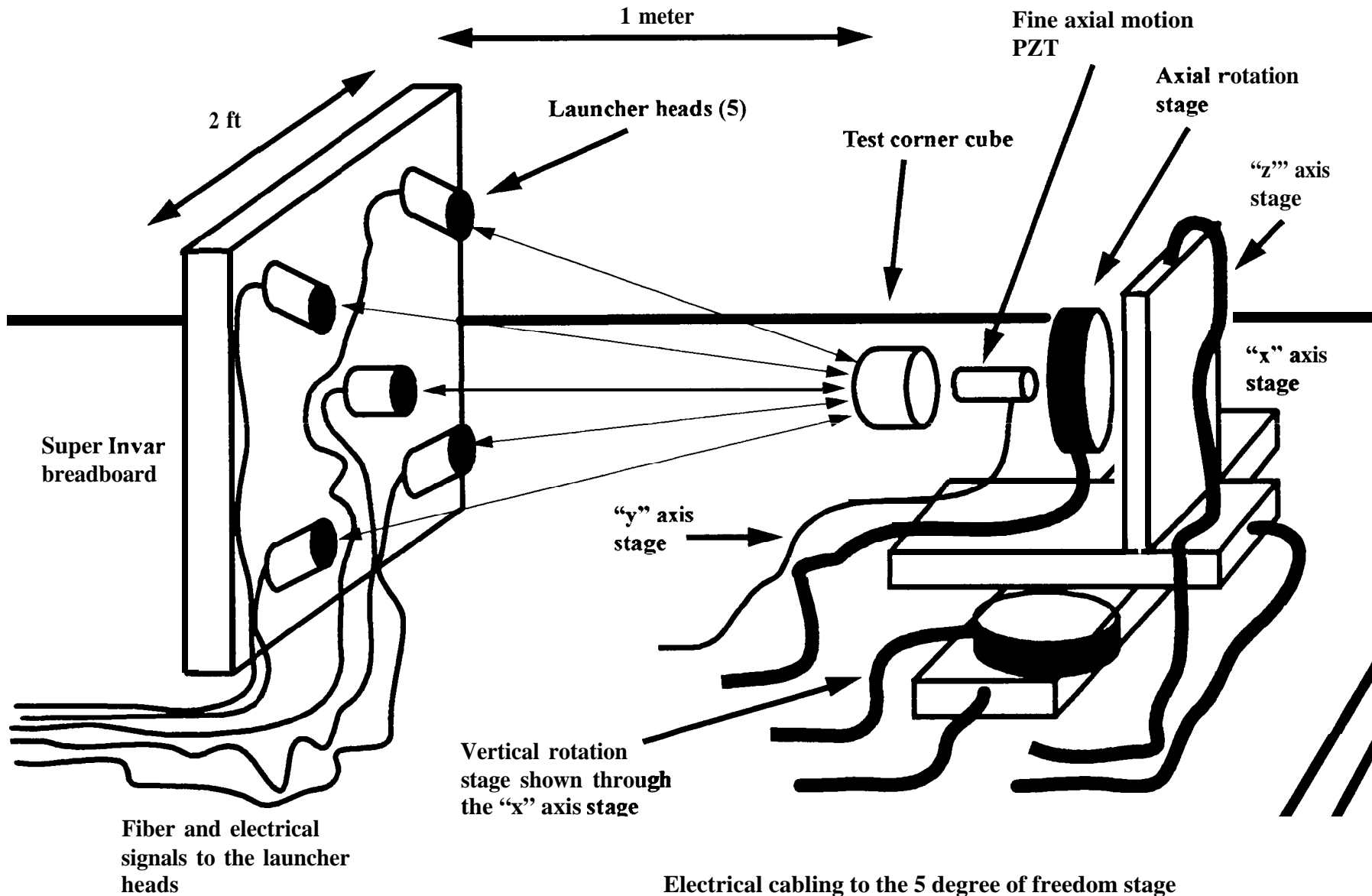


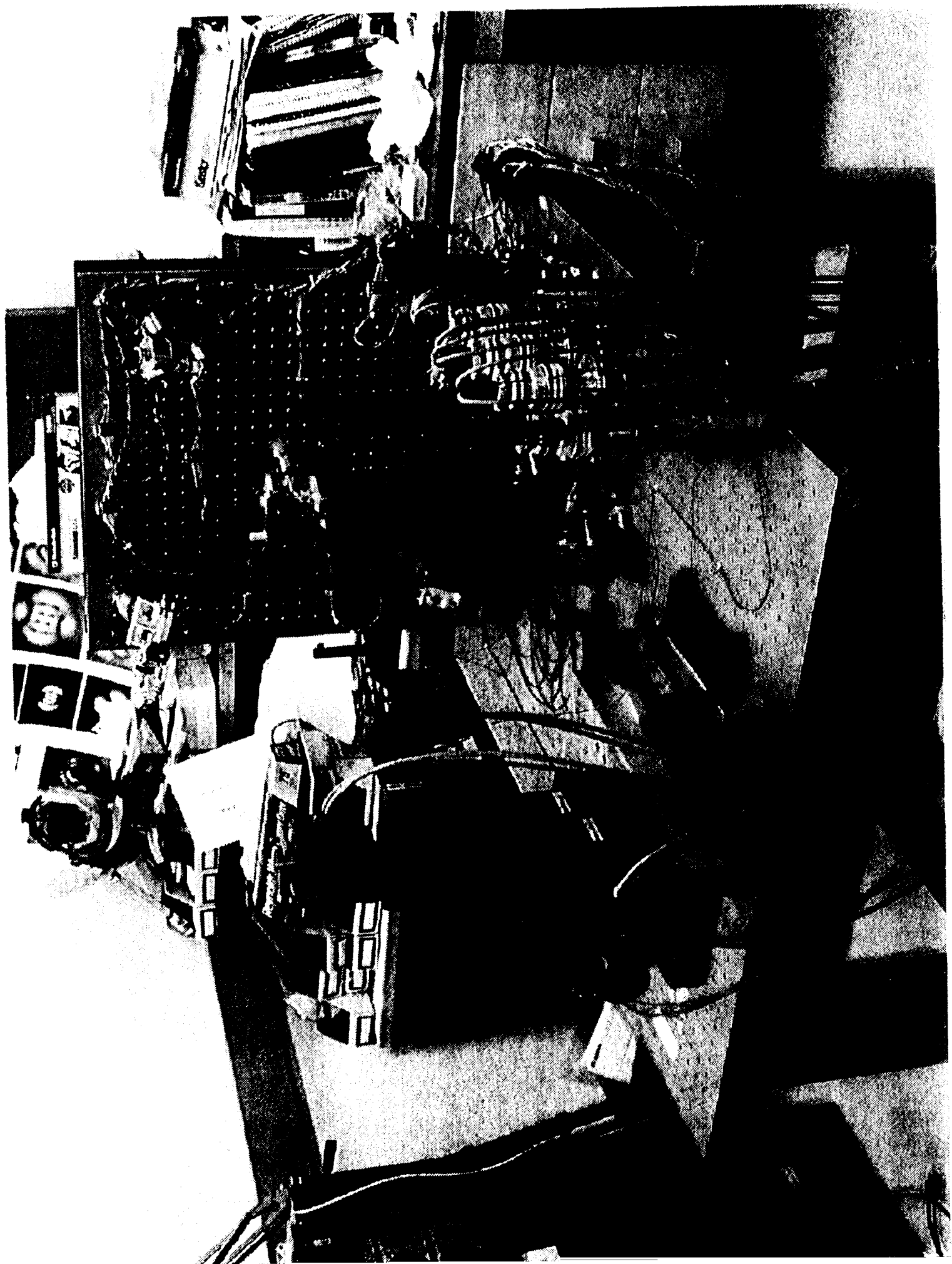
PICOMETER METROLOGY

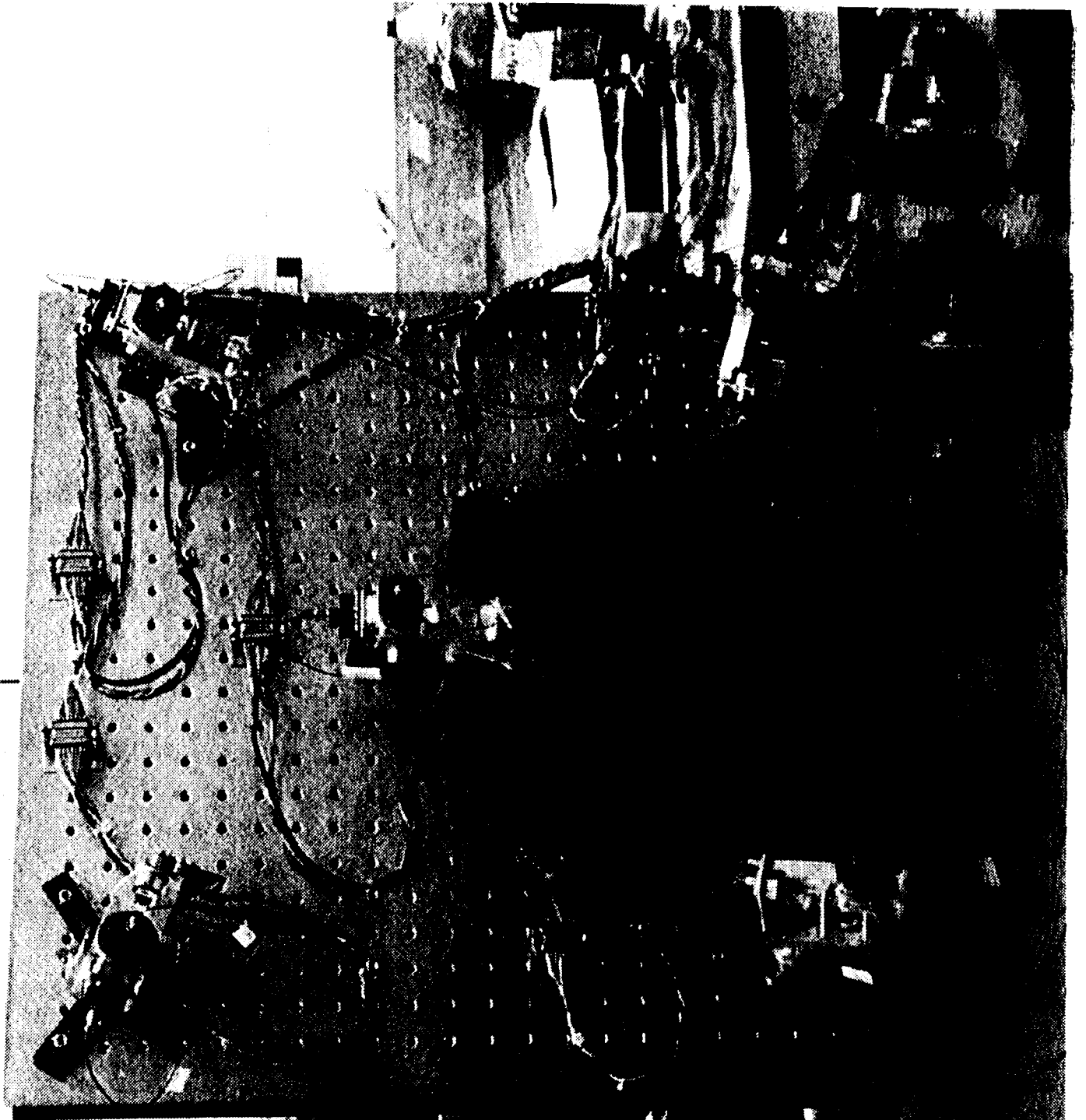
- Picometer metrology experiments are conducted in vacuum to avoid the effects of atmospheric turbulence and varying temperature.
- Four different metrology experiments are conducted:
 - The RELATIVE metrology gauge
 - The SURFACE metrology gauge
 - The ABSOLUTE metrology gauge
 - The 3- σ metrology gauge

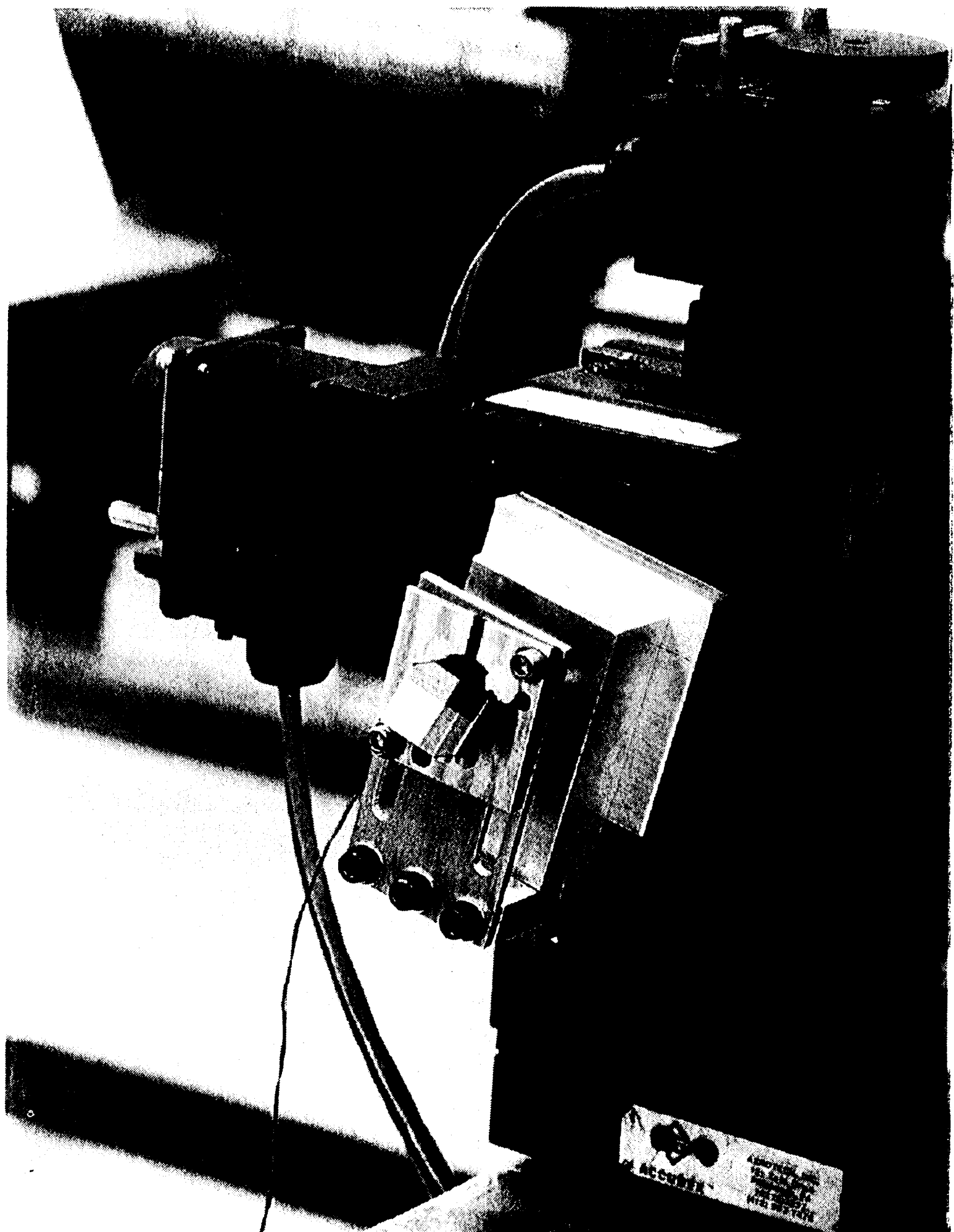
3-D METROLOGY

3D METROLOGY EXPERIMENT CONFIGURATION

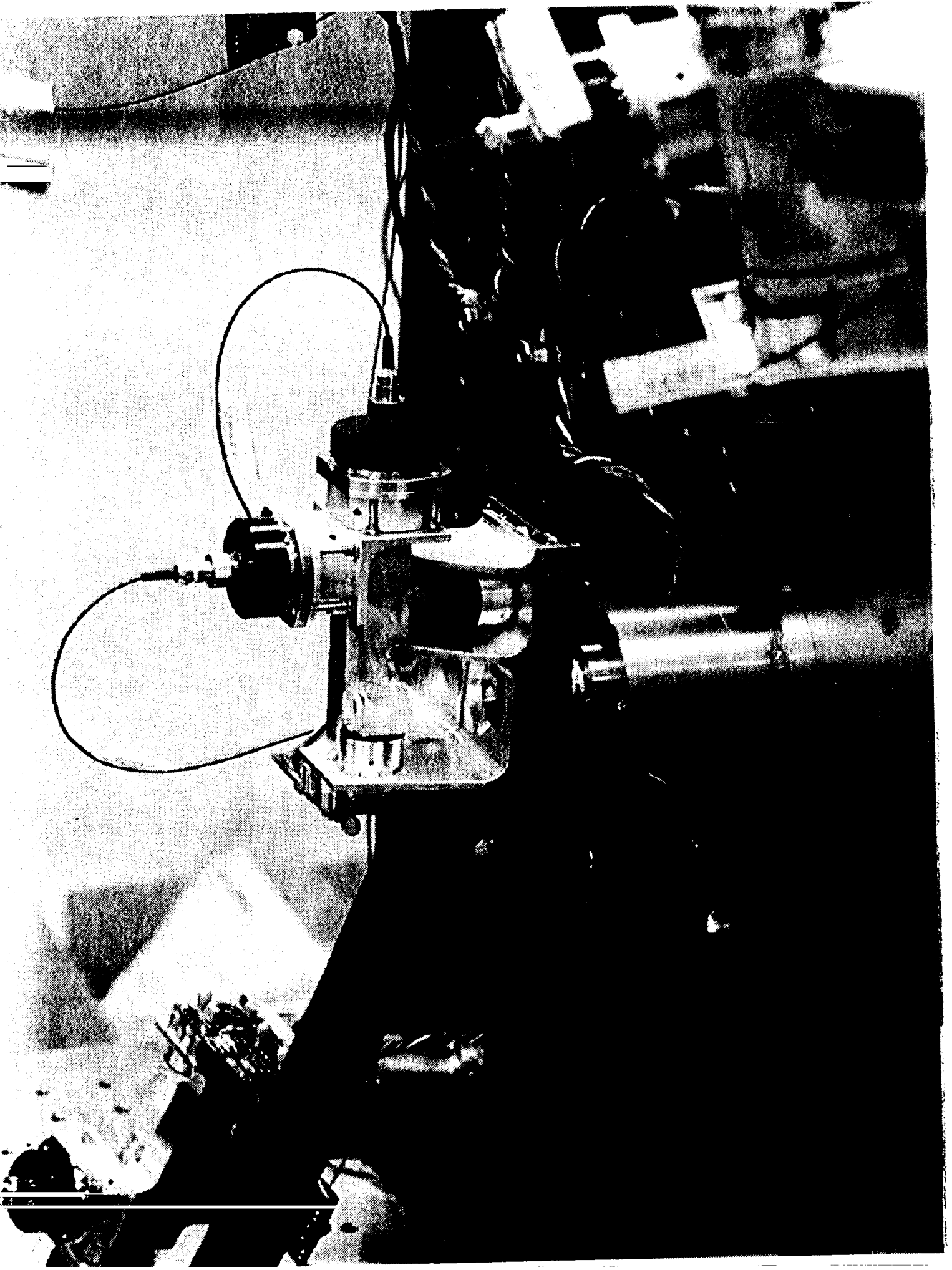


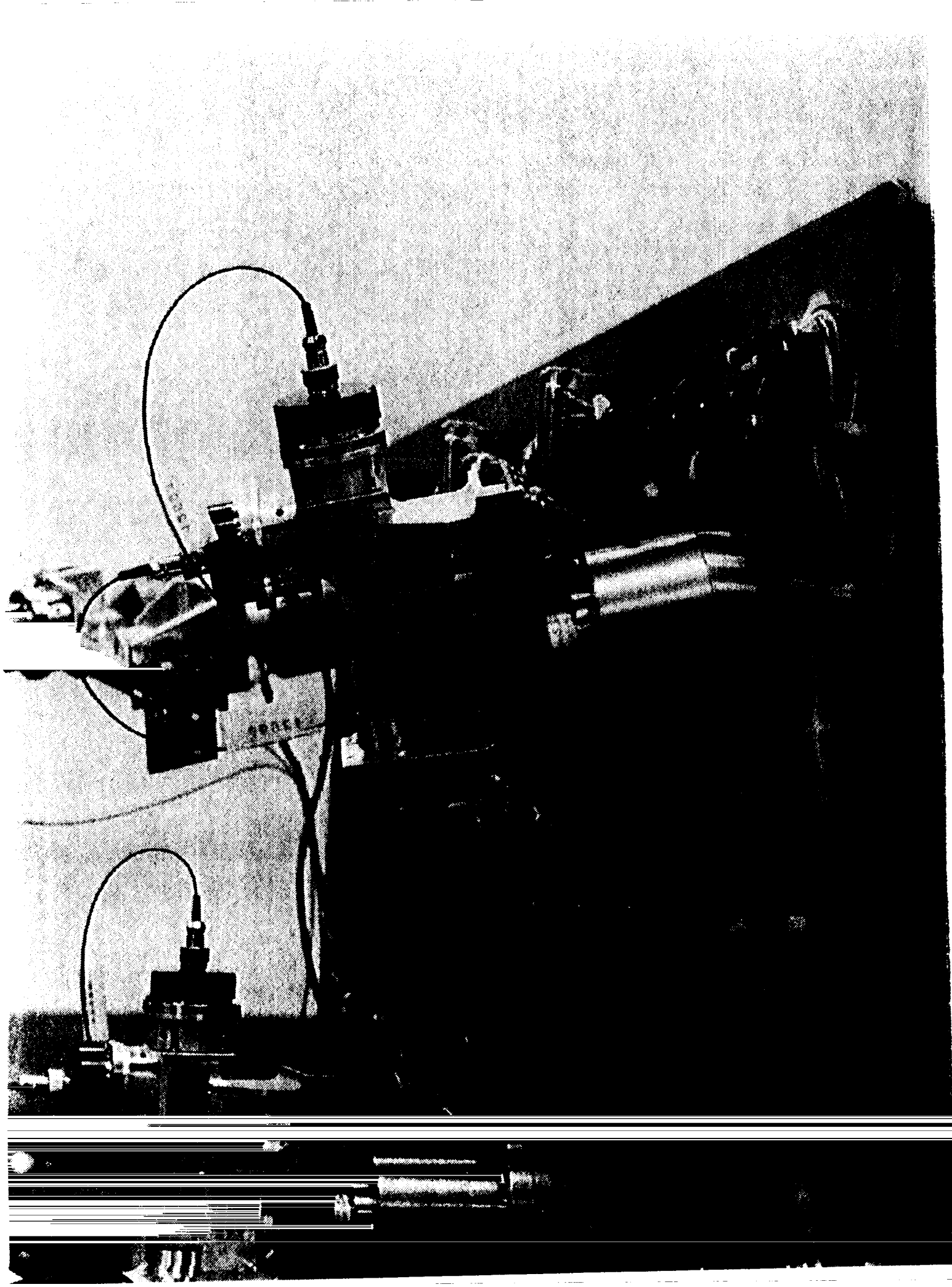


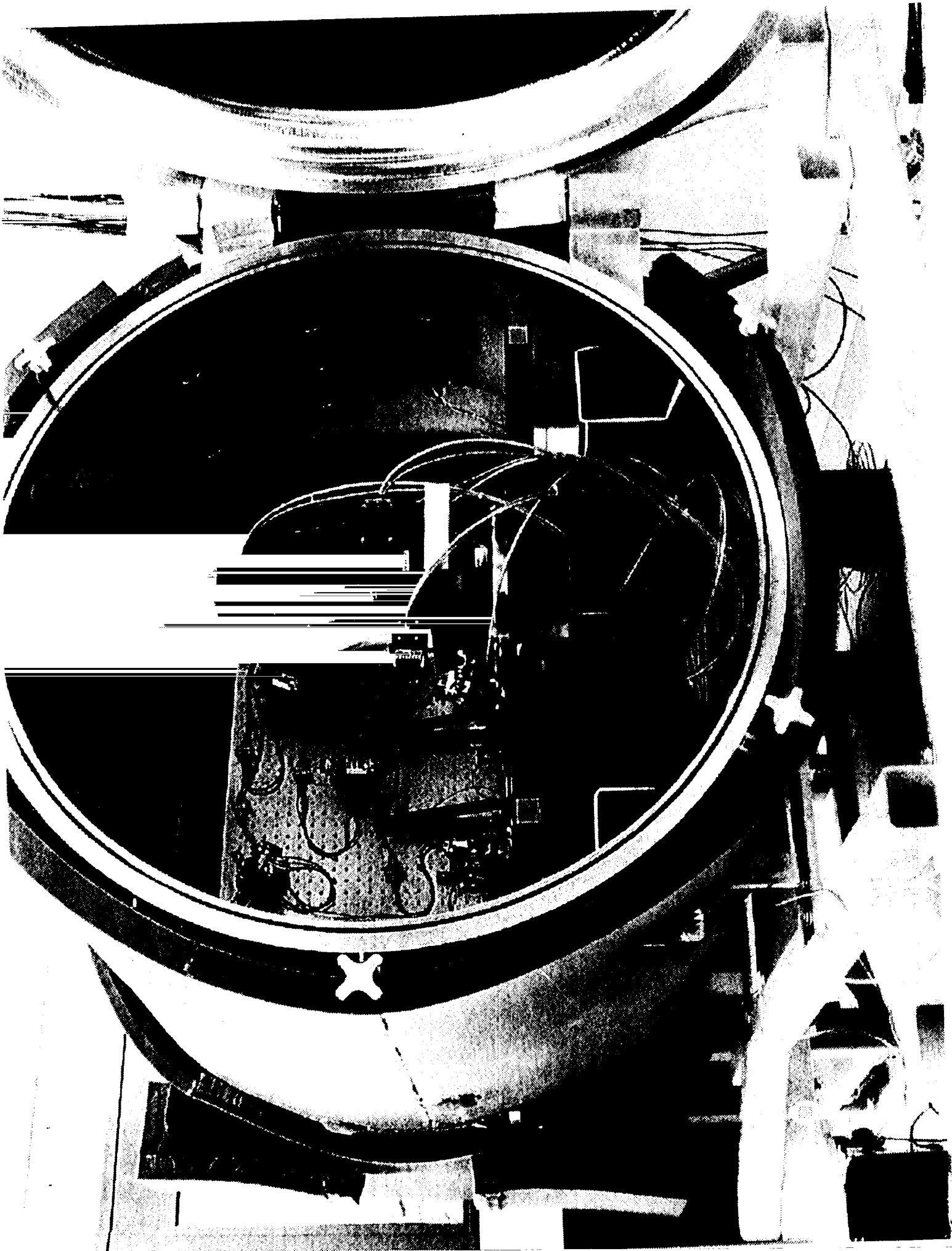


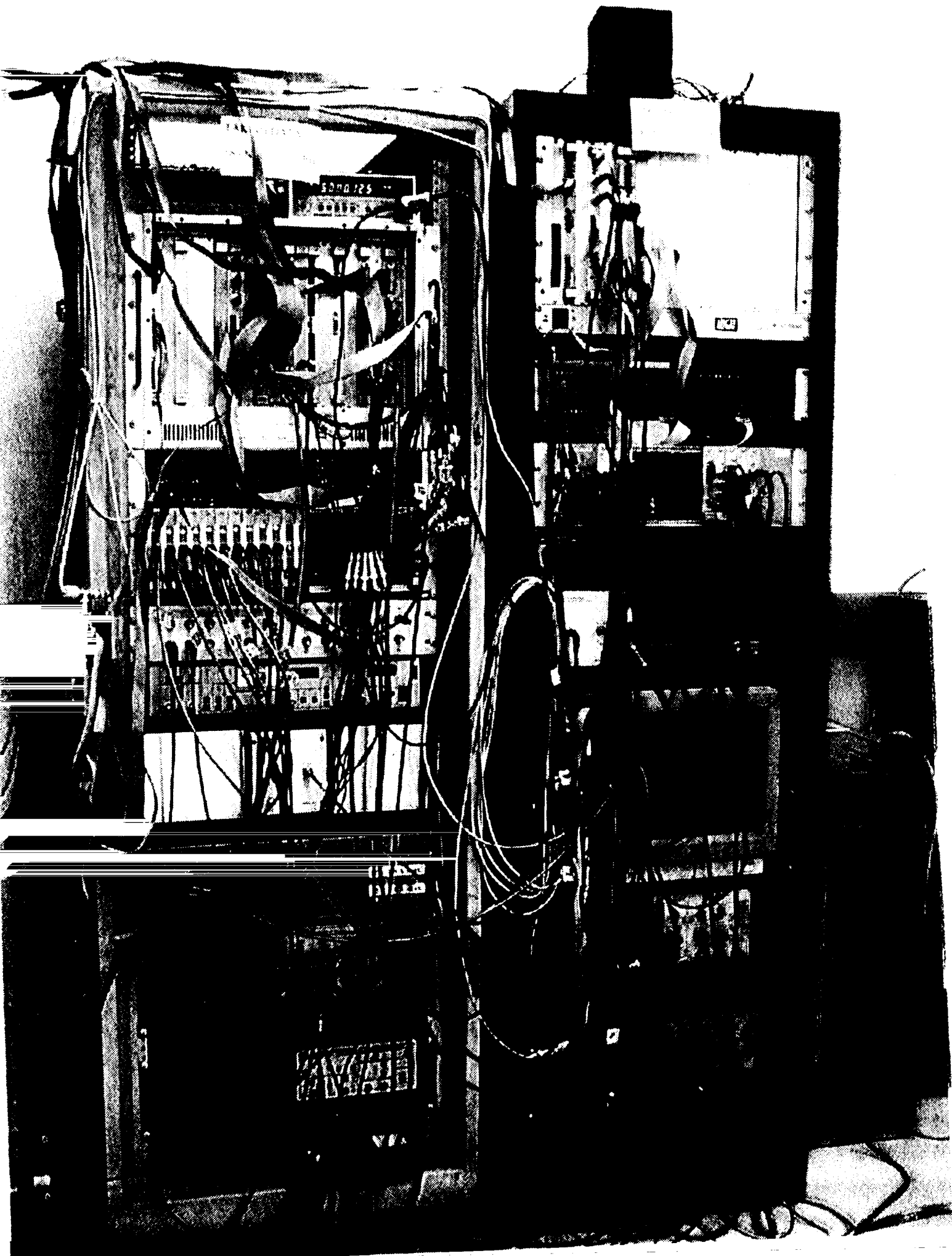


ACCURATE
APPROXIMATE
FOR ALL USES
FOR ALL USES
FOR ALL USES
FOR ALL USES

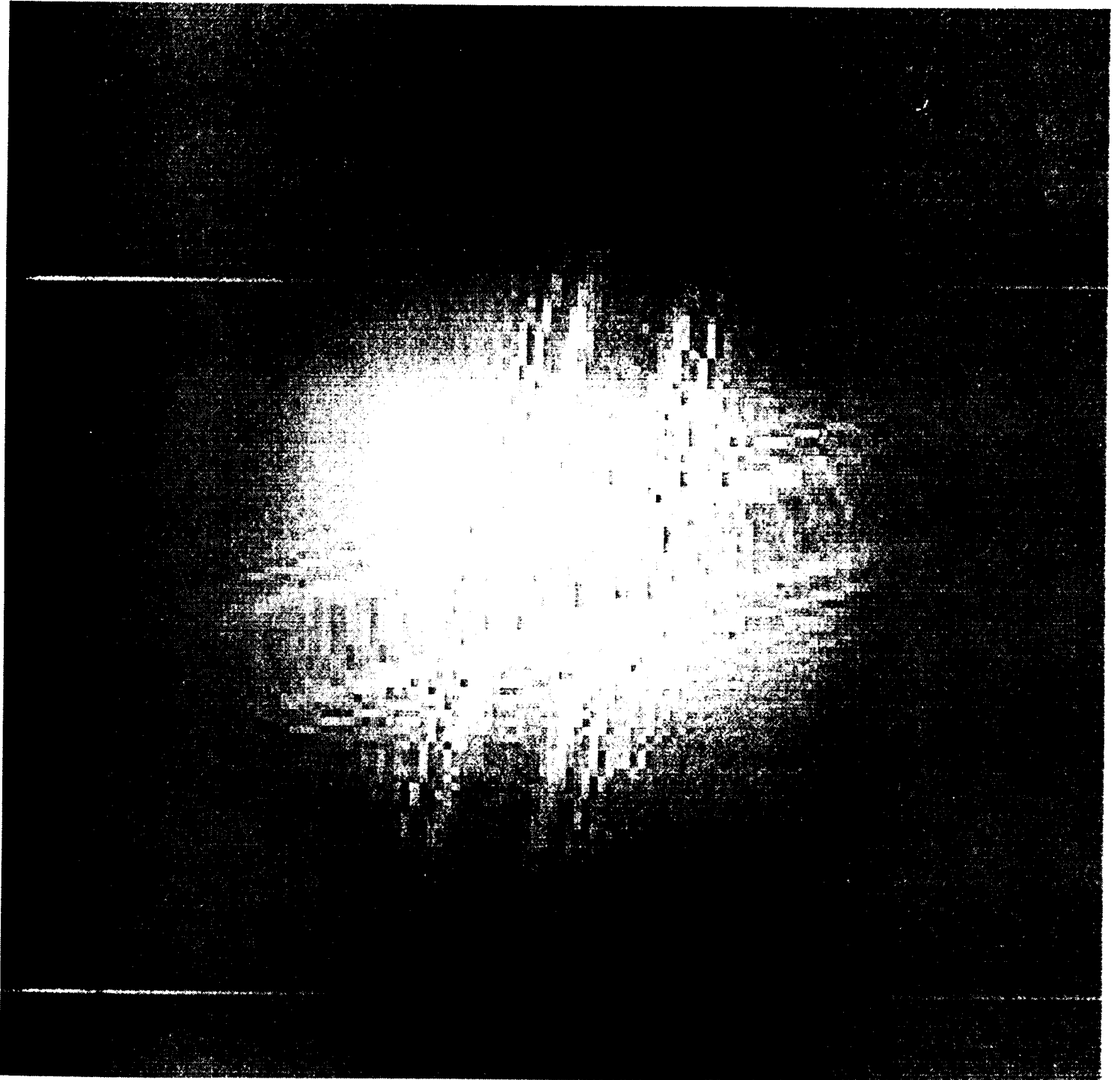








RETRO-REFLECTOR INDUCED
ABERRATIONS



91 / 20 / 10

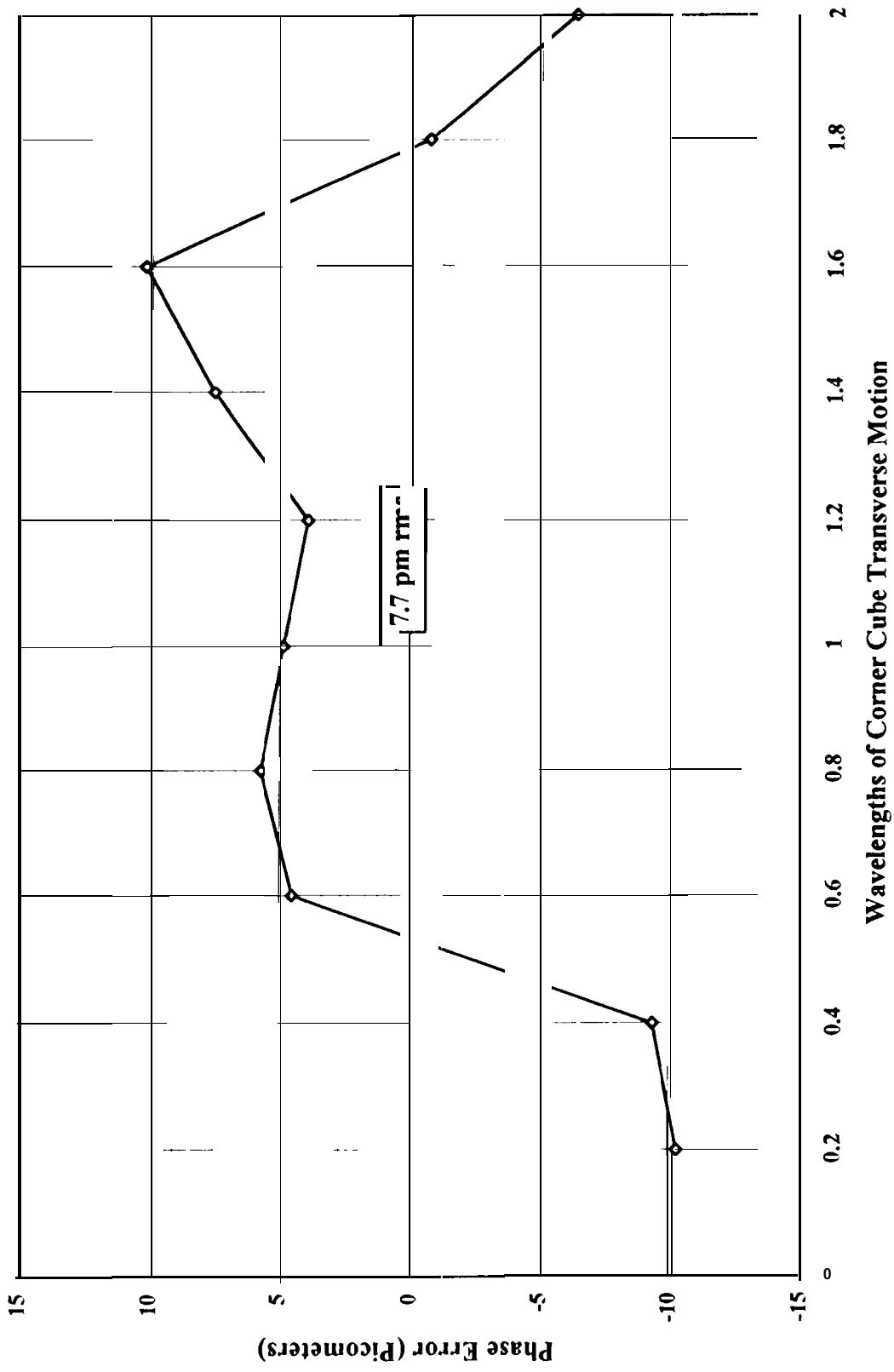
Albert Einstein

BA

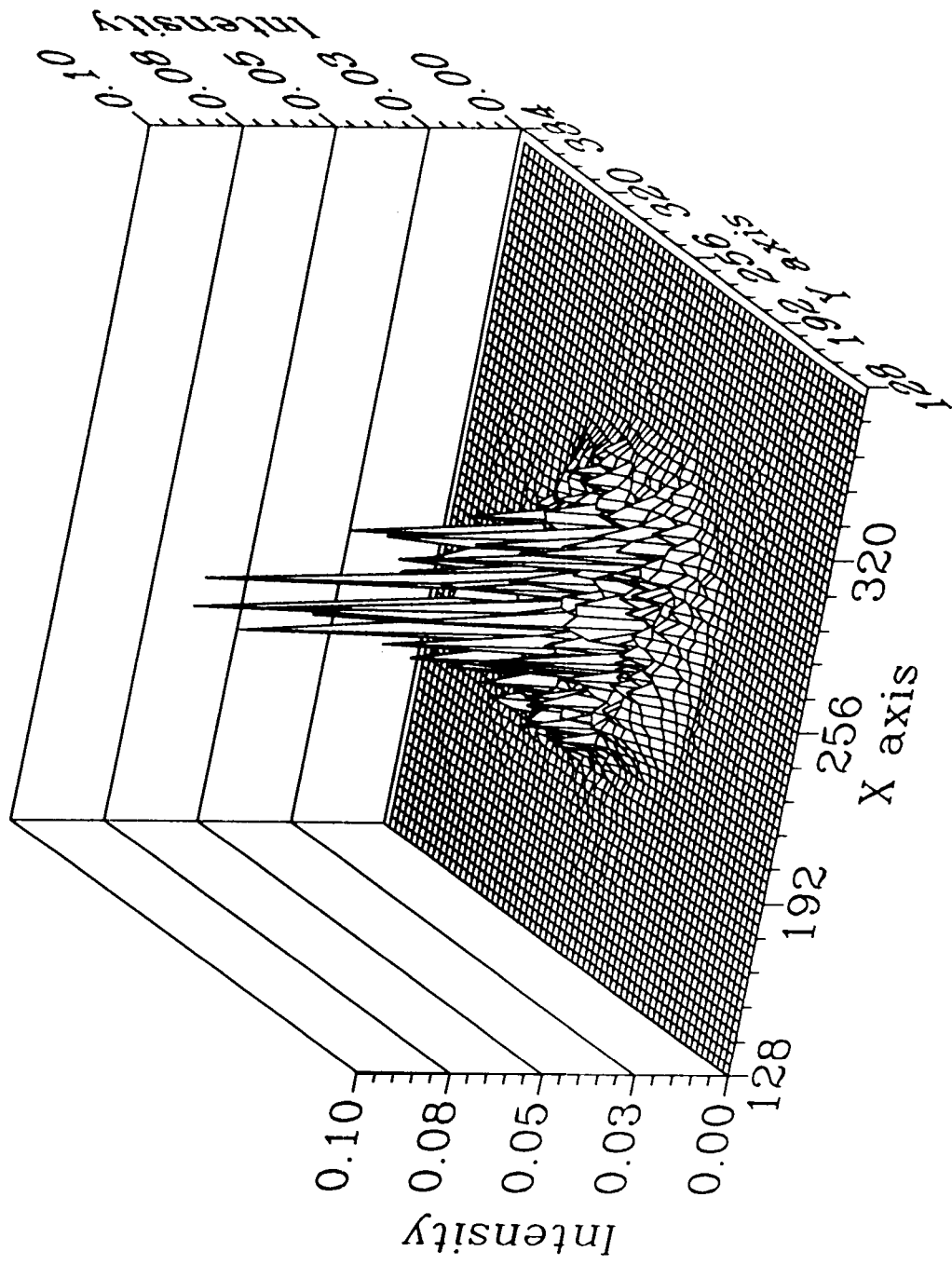
1921

Handwritten signature

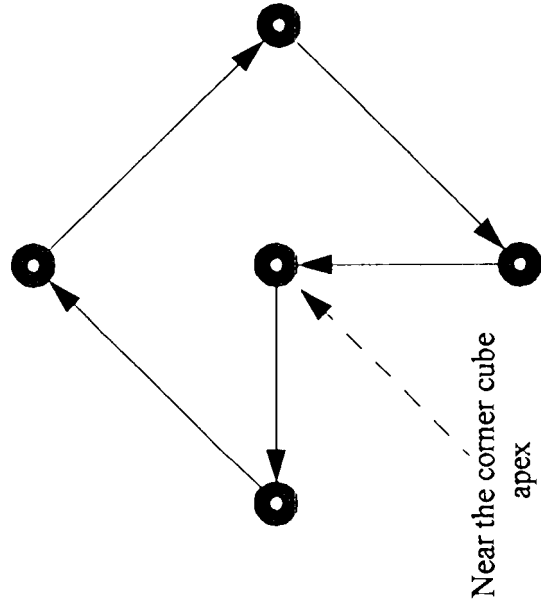
The Effect of Corner Cube Imperfections On the Detected Phase



Orthogonal Intensity (10^4)

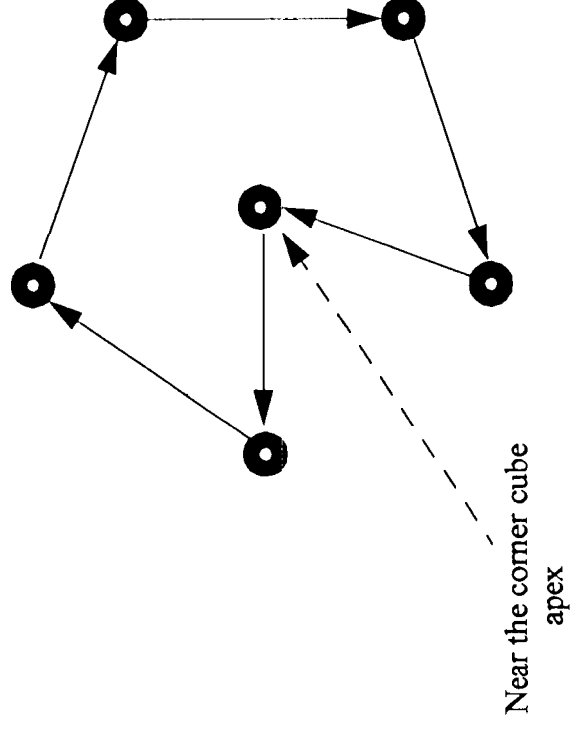


DITHERING RESULTS



Near the corner cube
apex

5 point dither pattern

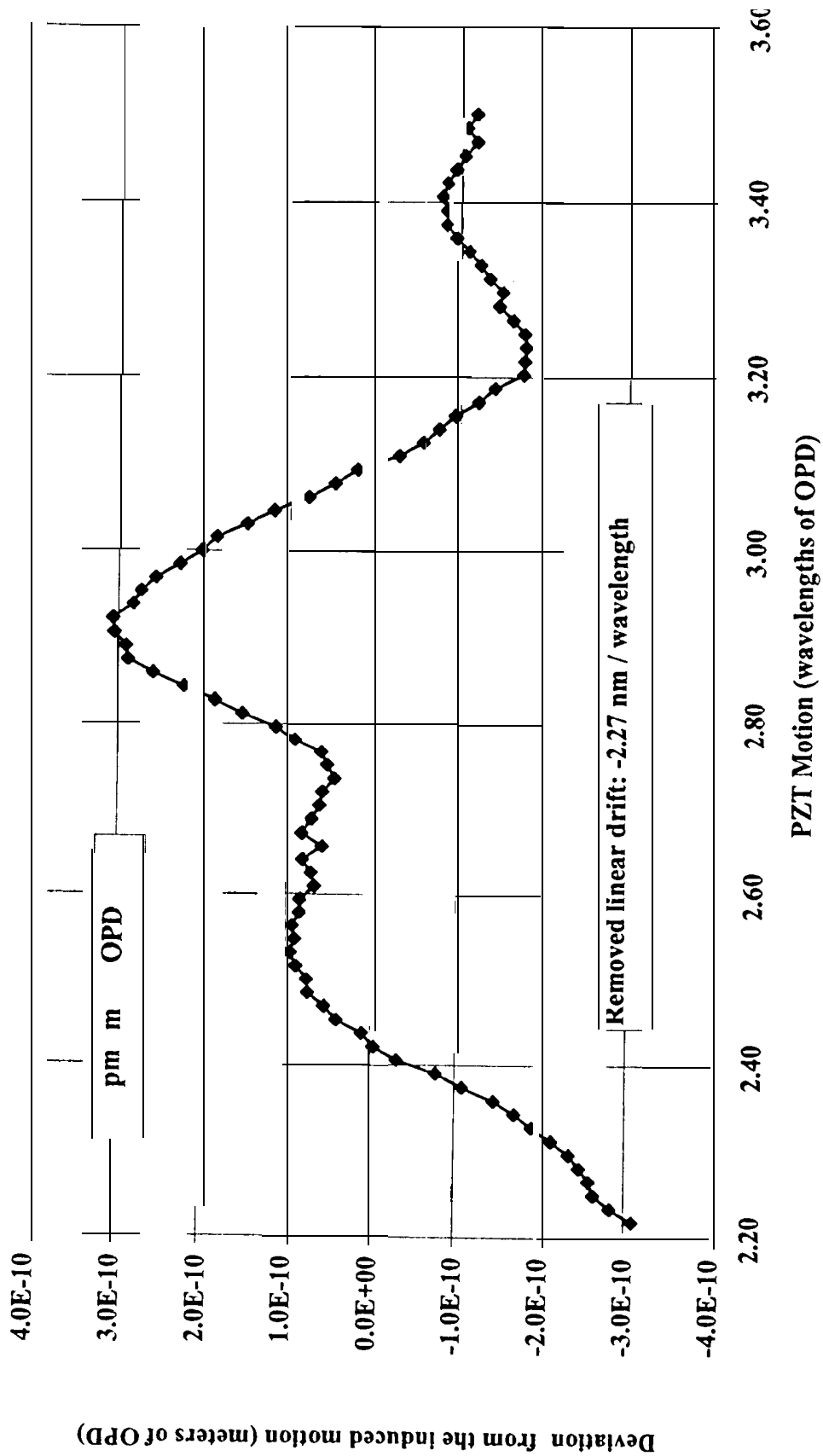


Near the corner cube
apex

6 point dither pattern

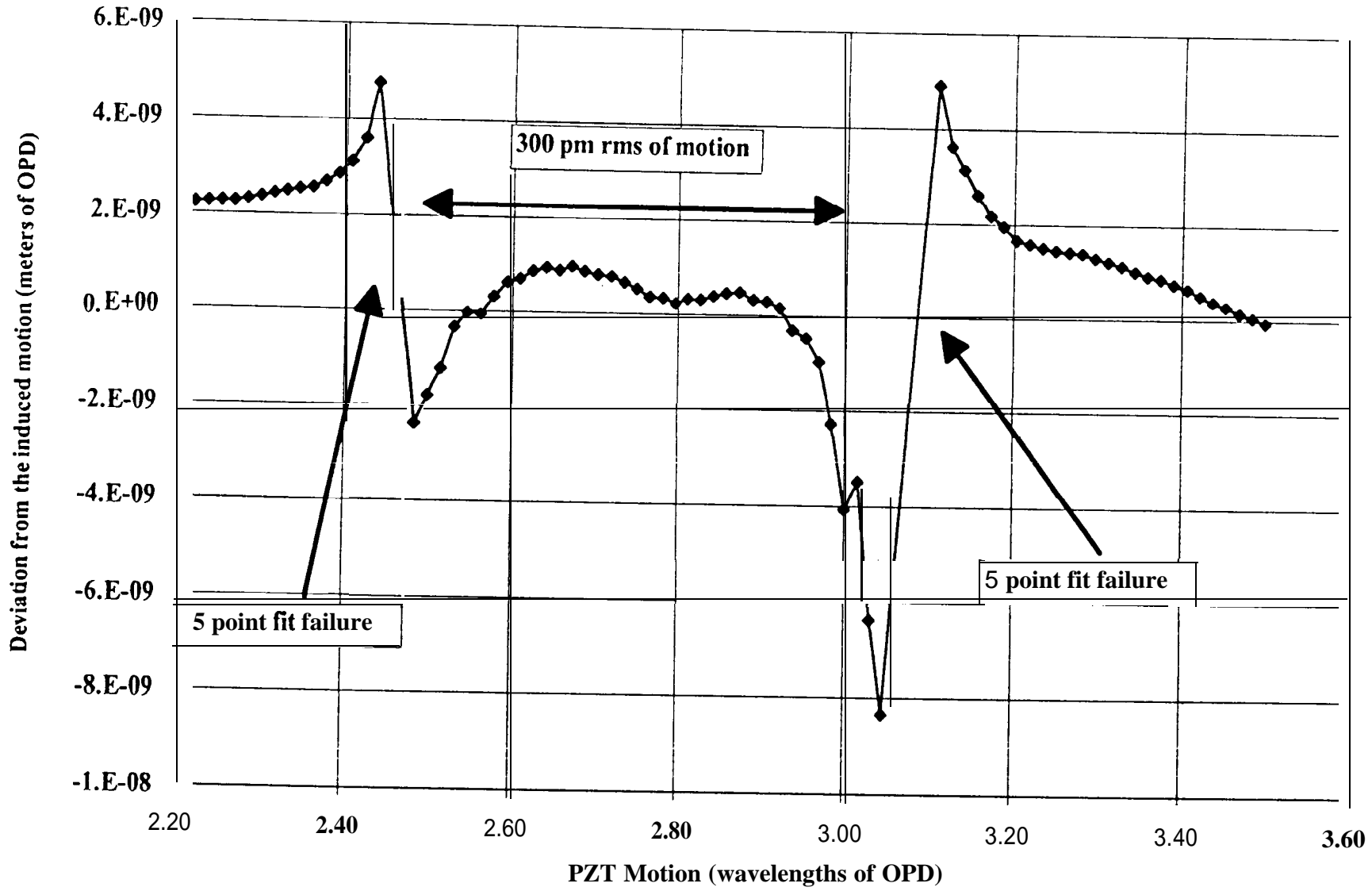
genta
12/11/1996

3 D Metrology, Head #1 tracking Head #5 in air (12/03/1996)
After two cyclic averages, no parabolic fit
A linear drift is removed

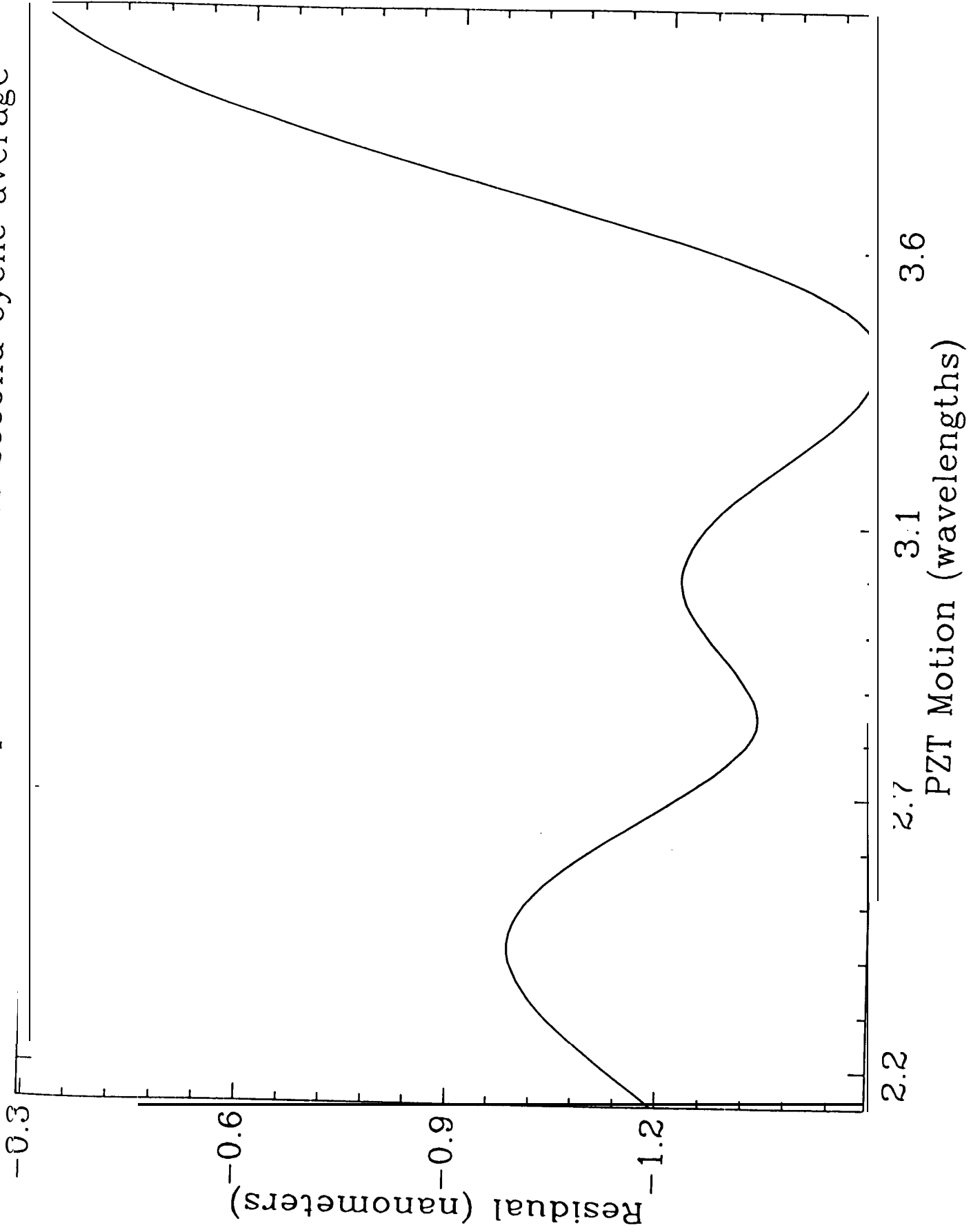


12/11/1996

3 D Metrology, Head #1 tracking head #5 in air (12/03/1996)
After two cyclic averages and parabolic fitting
No linear term removed.

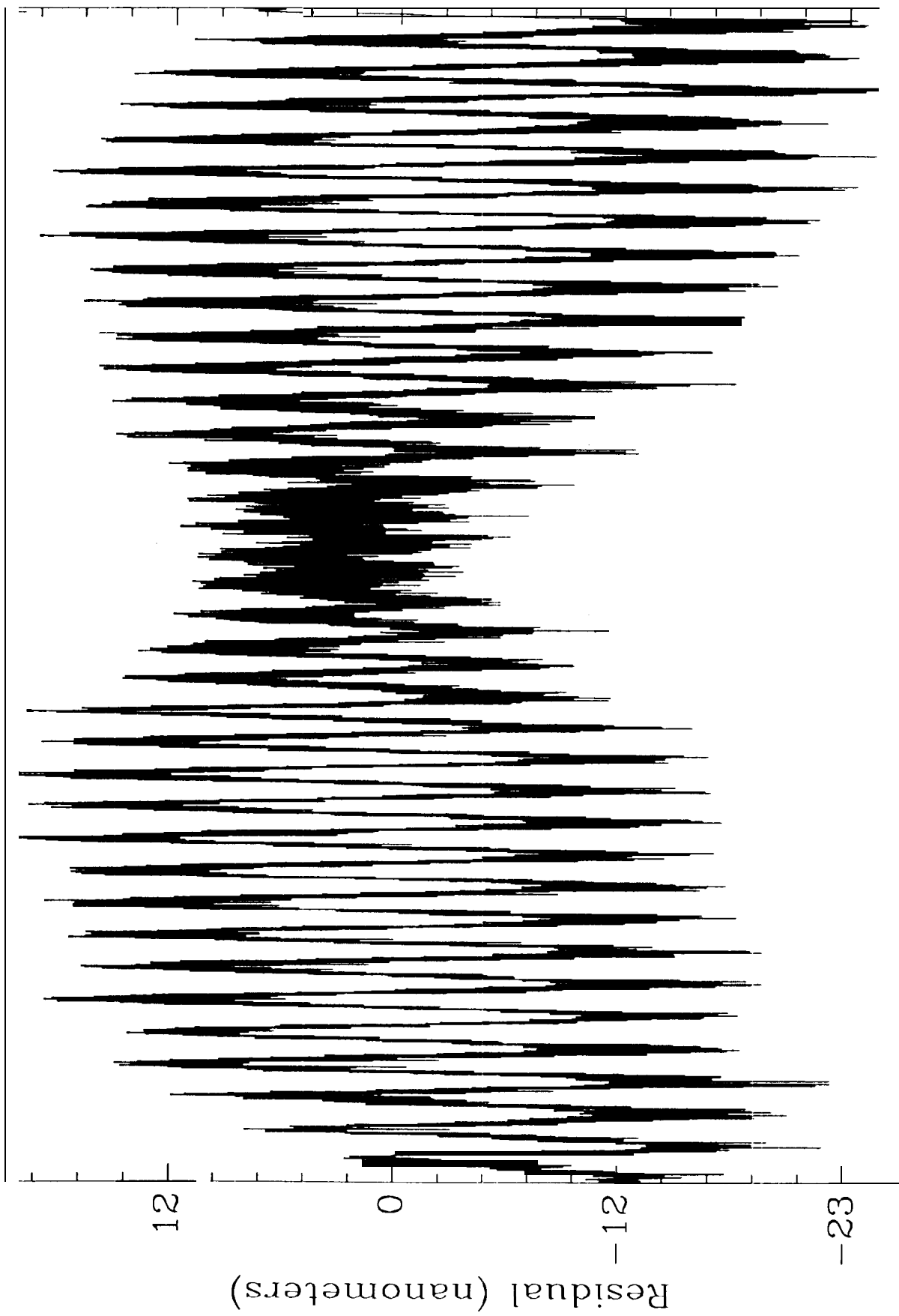


Residual after quadratic fit to second cyclic average



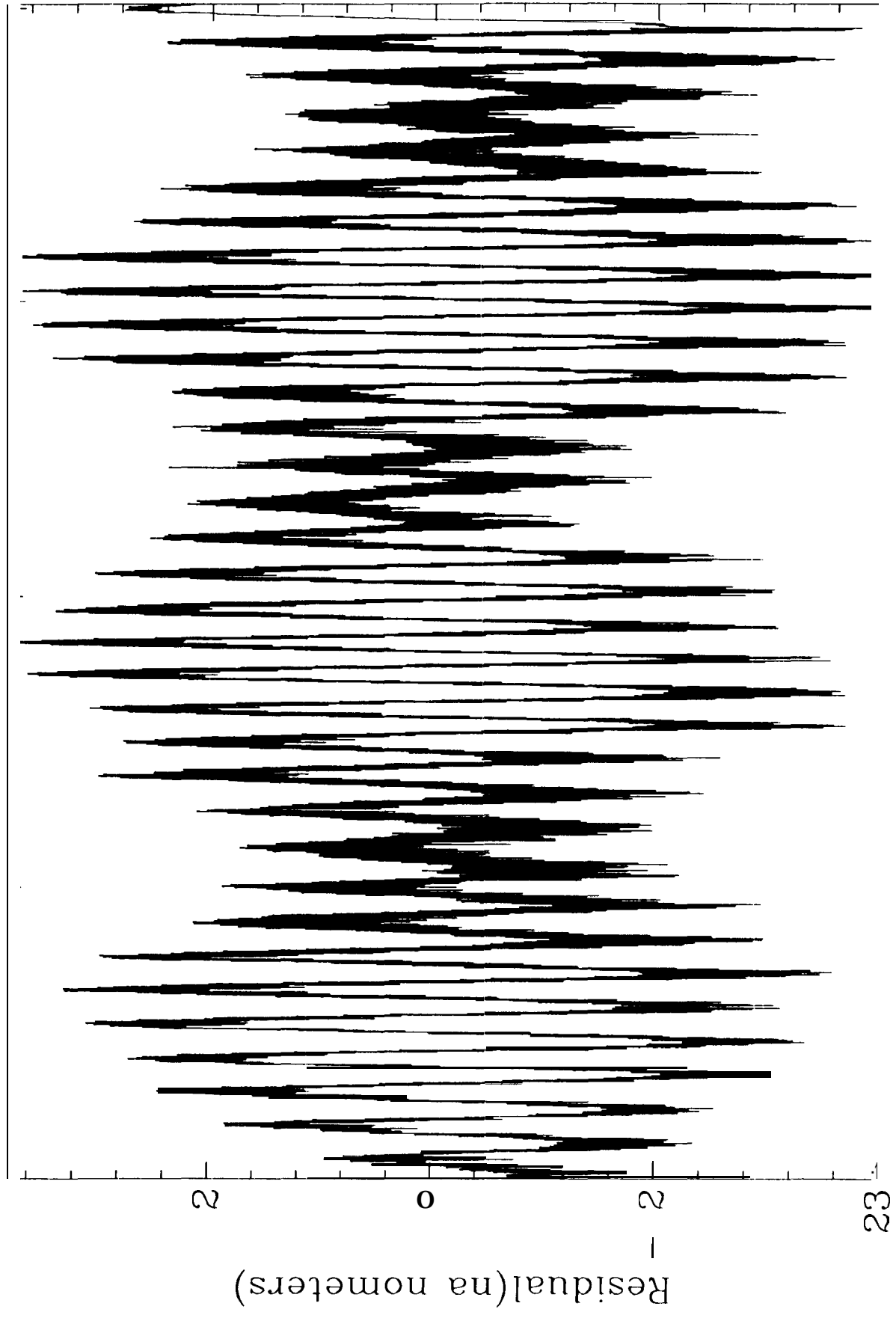
EFFECT OF RETRO-REFLECTOR
DEFECTS **ON** POLARIZATION

Residua after PZT motion fit



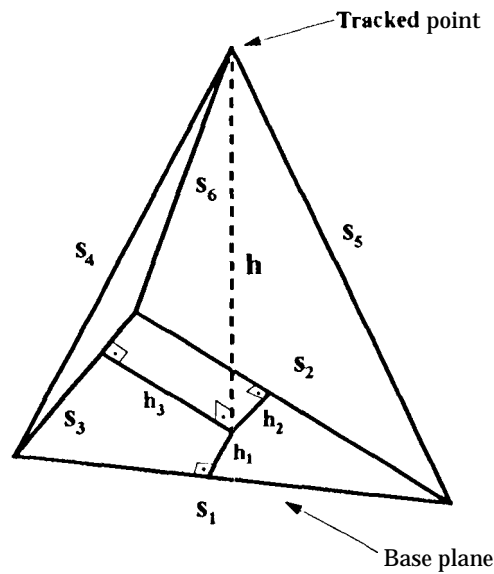
9.2 18.4 27.6 36.9
PZT Motion (wavelengths)

Residua after PZT motion fit



9 2 18.4 27.6 36.9
PZT Motion (wavelengths)

3-DIMENSIONAL TRACKING IN AIR



$$h^2 = \frac{(-s_1^2 s_6^4 - s_1^2 s_5^4 - s_1^2 s_4^4 - s_2^4 s_4^2 - s_3^2 s_5^4 - s_3^4 s_5^2 - s_1^2 s_2^2 s_3^2 + s_1^2 s_2^2 s_4^2 + s_1^2 s_2^2 s_6^2 + s_1^2 s_3^2 s_5^2 + s_1^2 s_3^2 s_6^2 - s_1^2 s_4^2 s_5^2 + s_1^2 s_4^2 s_6^2 + s_1^2 s_5^2 s_6^2 + s_2^2 s_3^2 s_4^2 + s_2^2 s_3^2 s_5^2 + s_2^2 s_4^2 s_5^2 + s_2^2 s_4^2 s_6^2 - s_2^2 s_5^2 s_6^2 + s_3^2 s_4^2 s_5^2 - s_3^2 s_4^2 s_6^2 + s_3^2 s_5^2 s_6^2)}{d^2},$$

where d is given by:

$$d = -s_1^4 - s_2^4 - s_3^4 + 2s_1^2 s_2^2 + 2s_1^2 s_3^2 + 2s_2^2 s_3^2.$$

Note that $d = 4 \times \text{Area of the triangle } (s_1, s_2, s_3)$. The coordinate lengths h_1 , h_2 and h_3 are given by:

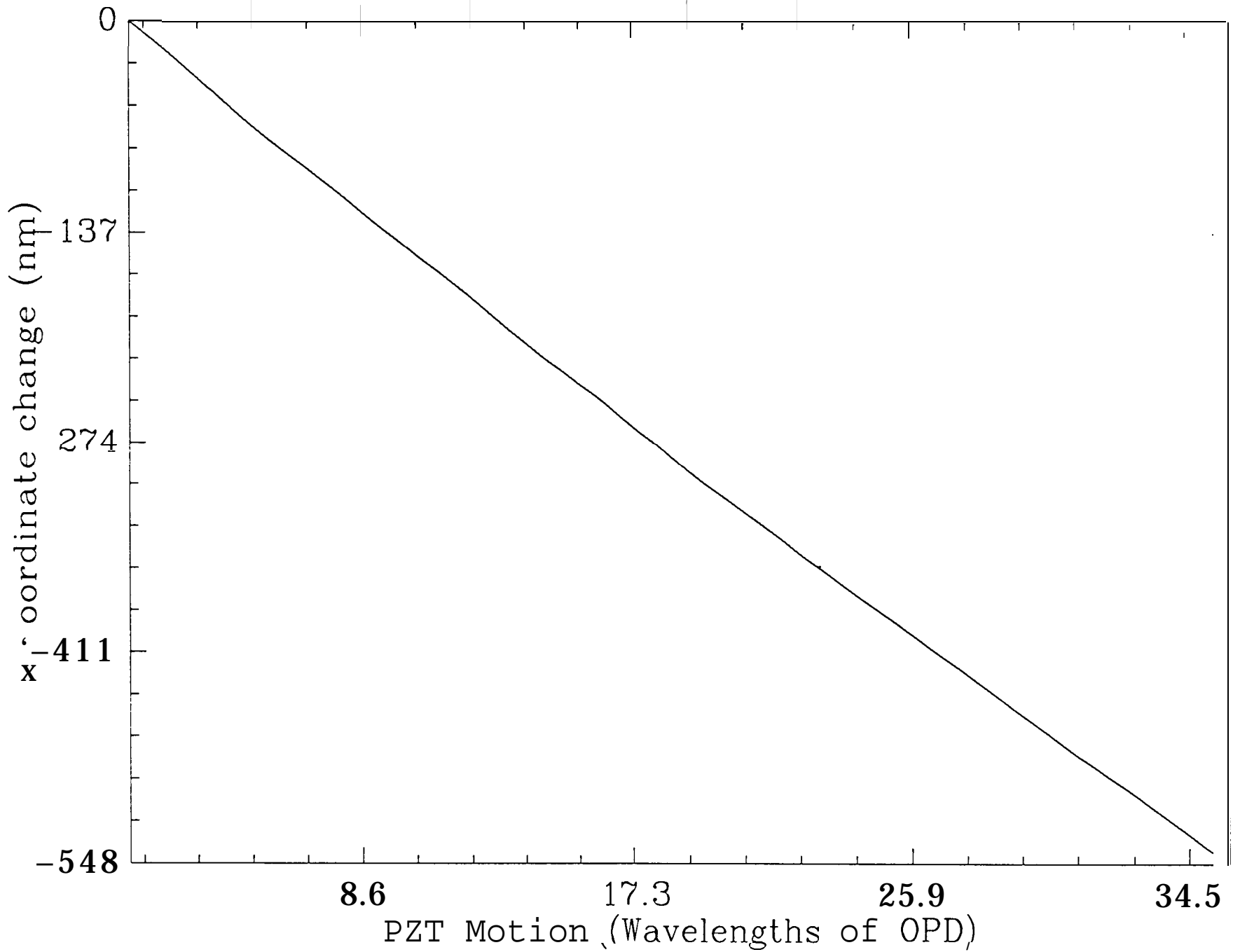
$$h_1 = (2s_1^2(s_2^2 + s_5^2 - s_6^2) - (s_1^2 + s_2^2 - s_3^2)(s_1^2 - s_4^2 + s_5^2))/2s_1 d,$$

$$h_2 = (2s_2^2(s_3^2 - s_4^2 + s_6^2) - (s_2^2 + s_3^2 - s_1^2)(s_2^2 - s_5^2 + s_6^2))/2s_2 d,$$

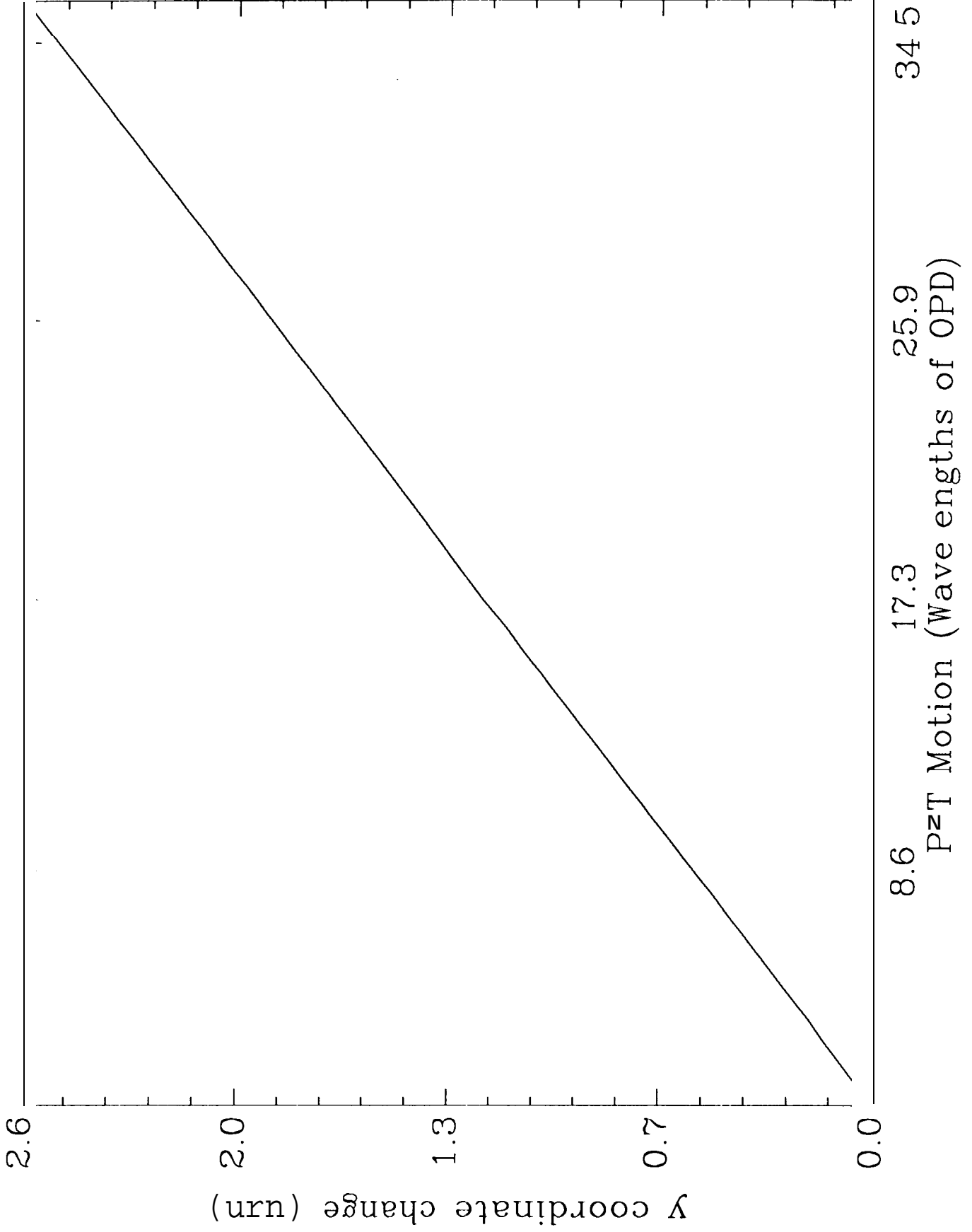
$$h_3 = (2s_3^2(s_2^2 - s_5^2 + s_6^2) - (s_2^2 + s_3^2 - s_1^2)(s_3^2 - s_4^2 + s_6^2))/2s_3 d,$$

THE COMPLETE SOLUTION TO THREE DIMENSIONAL SURVEYING

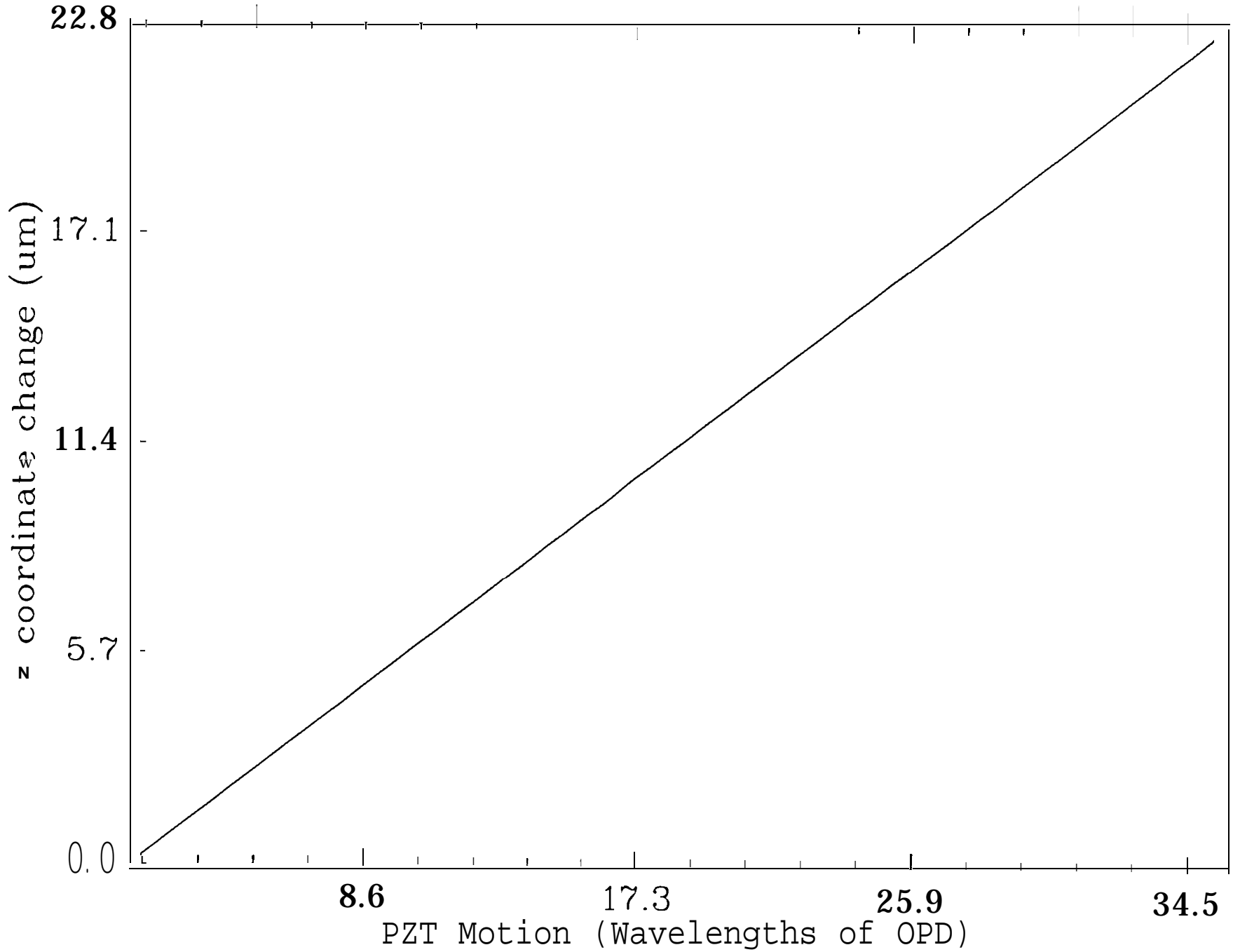
X Coordinate Change:



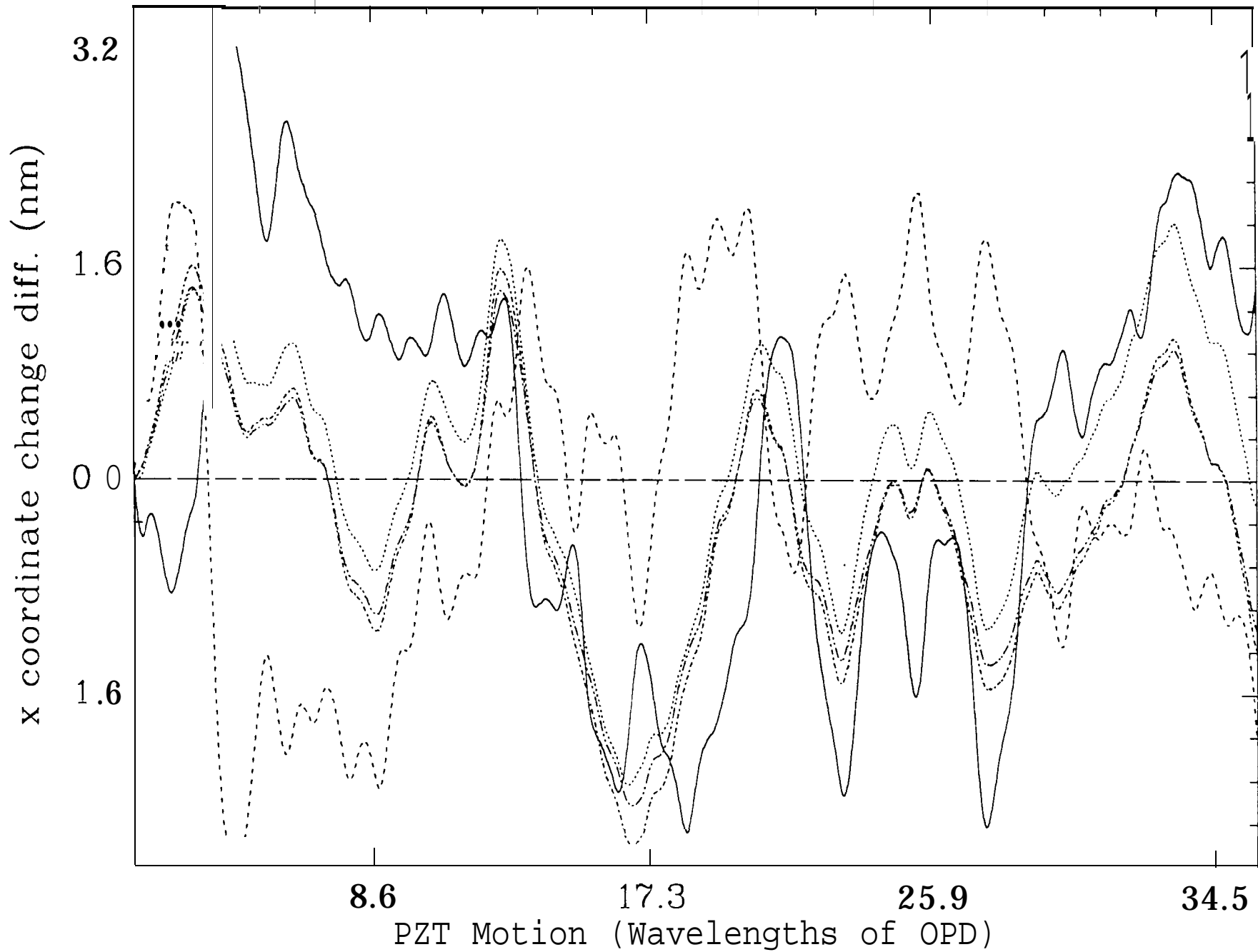
Y Coordinate Change:



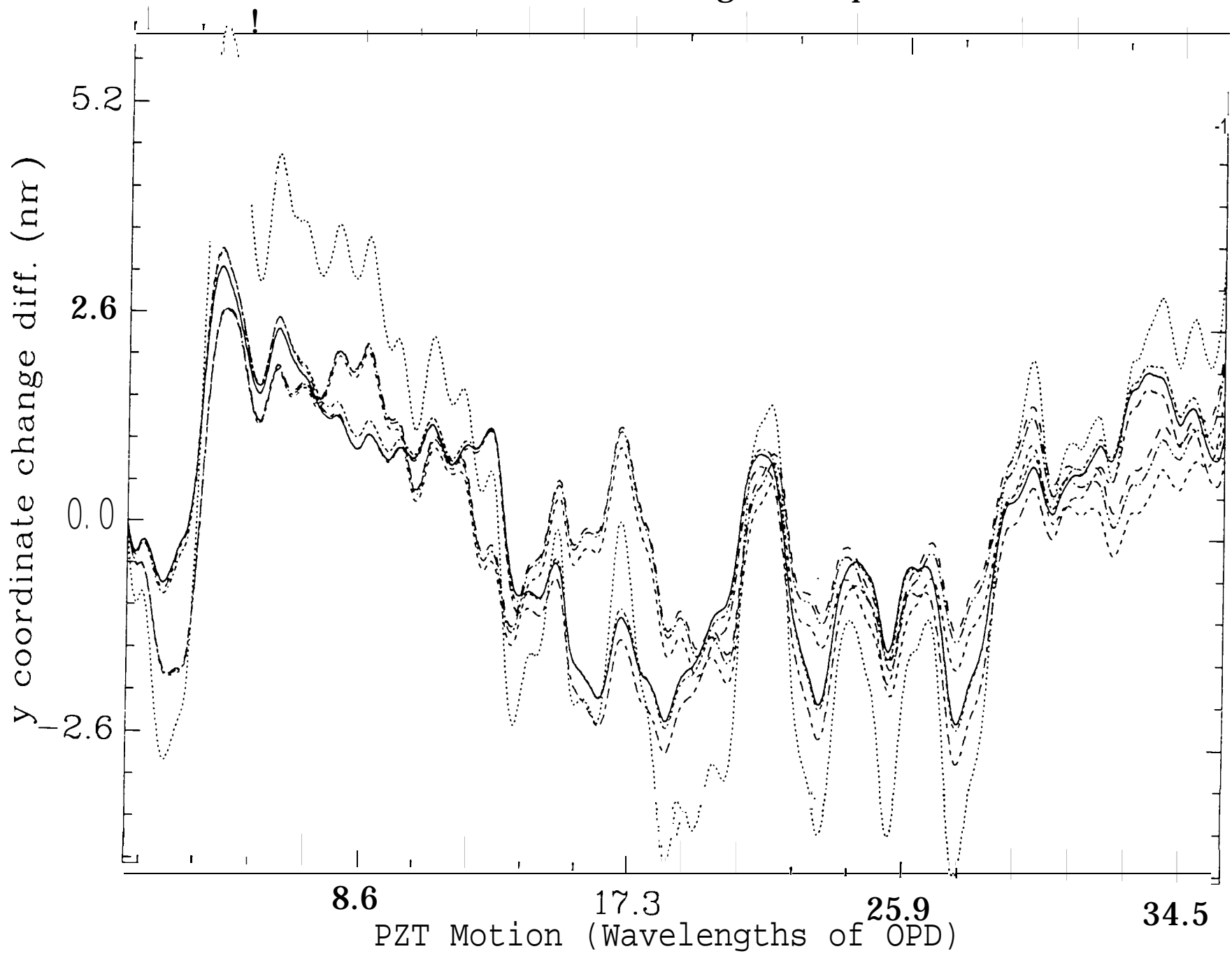
Z Coordinate Change:



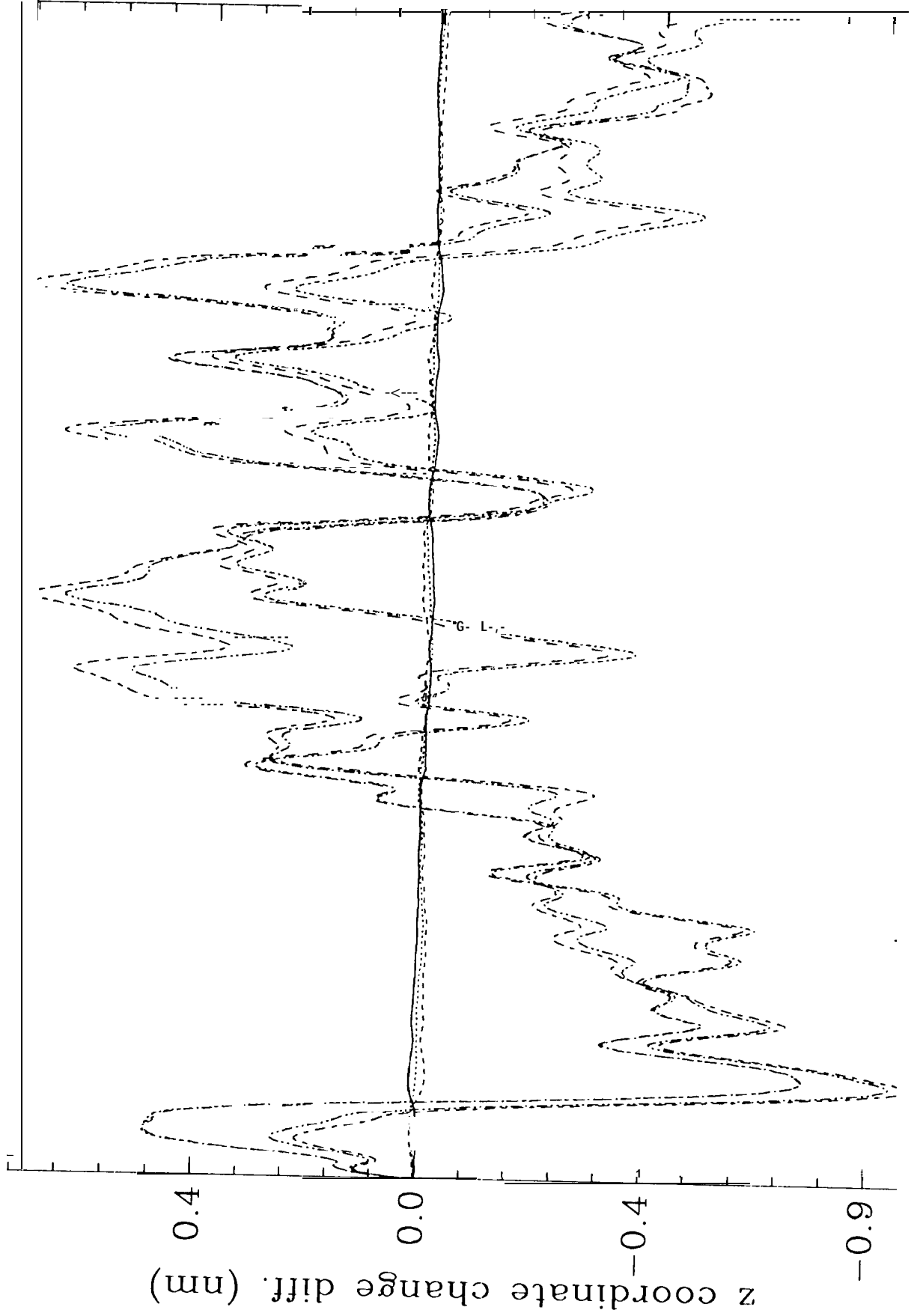
X Coordinate Change Comparison:



Y Coordinate Change Comparison:



Z Coordinate Change Comparison:



0.0 17.3 25.9 34.5
PZT Motion (Wavelengths of OPD)

SUMMARY

- **A simulation showing the effects of imperfect open-faced corner cube retro-reflectors is presented. For well made cubes, and for large enough input beams, the detected phase errors are less than 30 picometers as the cube moves transverse to the input beam by a few wavelengths of light.**
- . **Heterodyne gauge data showing the effects of the corner cube defects on the polarization of the reflected beams is shown.**
- **Simple analytical tracking formulas for 3-dimensional metrology is given.**
- . **Tracking performance of the 3-dimensional metrology gauge in still air without absolute metrology, but with a crude initial survey is presented. When the final head positions as well as the total motion is solved for, the residual disagreement between all tetrahedral is below one nanometer for about 10 wavelengths of OPD of total motion. For larger excursions, the disagreement is below 2 nm peak.**

NEXTSTEPS

- **Larger total motions result in more accurate determinations of the base geometry. These are implemented using the motion stages. The resulting total motion will be 100 times larger, enabling us to determine the base geometry with sub-millimeter accuracy.**
- **Absolute metrology gauges on the five out-of-base-plane lengths will increase the accuracy of the base geometry solution even further as only one parameter needs to be solved for with this arrangement.**
- **Finally, in vacuum operation will remove all air turbulence and immensely improve the temperature stability. With the high speed scanning system, the location of the tracked virtual corner is more accurately determined by performing a raster scan of the apex area of the corner cube.**
- **The combined steps above will enable us to finally reduce the tracking error to tens of picometers.**